SMART SWITCHABLE BEAM ANTENNAS FOR INTERNET OF THINGS APPLICATIONS

A THESIS SUBMITTED TO
THE BOARD OF GRADUATE PROGRAMS
OF
MIDDLE EAST TECHNICAL UNIVERSITY, NORTHERN CYPRUS CAMPUS

BY

YEWANDE MARIAM ARAGBAIYE

IN PARTIAL FULFILLMENT OF THE REQUIREMENTS
FOR
THE DEGREE OF MASTER OF SCIENCE
IN ELECTRICAL AND ELECTRONICS ENGINEERING PROGRAM

SEPTEMBER 2021

ABSTRACT

SMART SWITCHABLE BEAM ANTENNAS FOR INTERNET OF THINGS APPLICATIONS

Yewande Mariam Aragbaiye
Master of Science, Electrical and Electronics Engineering Program
Supervisor: Assoc. Prof. Dr. Tayfun Nesimoğlu

September 2021, 91 pages

The main objective of this thesis is to design, fabricate and test novel and compact switchable and steerable beam smart antennas working at 2.4 GHz frequency that will be integrated to 6TiSCH networks for IoT applications.

In this thesis, two switchable beam antenna designs are presented. The first antenna design which is a dual-port multi-layered switchable beam antenna can steer and switch its main beam both in the azimuth and the elevation plane in four directions. A parasitic Yagi-Uda layer made up of copper strips serving as reflectors and directors is placed at an optimum distance above a square patch antenna. As a result of its high inter-port isolation, the proposed novel antenna is capable of transmitting and receiving RF signals simultaneously at the same frequency with a high gain of 6.19 dB to 6.28 dB respectively thus reducing the complexity of the antenna system.

The second antenna design presented is a 2x2 rectangular patch antenna array with an EBG structure at the ground plane. The antenna array consists of four rectangular microstrip patches all fed by using individual coaxial lines. The ground plane includes an EBG structure made up of square-shaped slots. The 2x2 antenna array can achieve beam steering angles from -36 to 36 degrees by changing the phase

and amplitude of the RF signal of the four coaxial ports. The inclusion of the EBG structure reduced the overall antenna size by 32.2%, it also improved the gain, bandwidth, and return loss properties of the antenna.

Keywords: Beam Steering, Electromagnetic Band-gap Structures, High Inter-port Isolation, Smart Antennas, Microstrip Antenna Array

ÖZ

ŞEYLERİN İNTERNETİ UYGULAMALARI İÇİN AKILLI DEĞİŞTİRİLEBİLİR HUZUN ANTENLERİ

Aragabiye, Yewande Mariam
Yüksek Lisans, Elektrik ve Elektronik Mühendisliği bölümü
Tez Yöneticisi: Assoc. Prof. Dr. Tayfun Nesimoğlu

Eylül 2021, 91 pages

Bu araştırmanın temel amacı, IoT uygulamaları için 6TiSCH ağlarına entegre edilecek 2.4 GHz frekansında çalışan yeni ve kompakt, anahtarlanabilir ve yönlendirilebilir huzmeli akıllı antenler tasarlamak, üretmek ve test etmektir.

Bu tezde, iki adet değiştirilebilir huzmeli anten tasarımı sunulmaktadır. Çift portlu çok katmanlı anahtarlanabilir huzme anteni olan ilk anten tasarımı, ana huzmesini hem azimutta hem de yükseklik düzleminde dört yönde yönlendirebilir ve değiştirebilir. Reflektör ve yönlendirici görevi gören bakır şeritlerden oluşan parazitik bir Yagi-Uda katmanı, kare bir yama anteninin üzerine optimum bir mesafeye yerleştirilmiştir. PIN diyot anahtarları ve iki besleme portu, reflektörlerin ve yönlendiricilerin uzunluğunu kontrol etmek için kullanılmıştır, böylece azimut düzleminde 360 ° kapsama ile dört yönde ışın değiştirme ve yönlendirme 2,4 GHz'lik çalışma frekansı korunarak elde edilmiştir. Önerilen yeni anten portlar arası izolasyonun yüksek olmasının bir sonucu olarak, aynı frekansta RF sinyallerini aynı anda sırasıyla 6.19 dB ile 6.28 dB'lik yüksek bir kazanç ile hem iletebilir hem de alabilir, böylece anten sisteminin karmaşıklığını azaltır.

Sunulan ikinci anten tasarımı, toprak düzleminde EBG yapısına sahip 2x2 dikdörtgen bir yama anten dizisidir. Anten dizisi, tümü ayrı koaksiyel hatlar

kullanılarak beslenen dört dikdörtgen mikroşerit yamadan oluşmaktadır. Toprak düzlemi, kare şekilli yarıklardan oluşan bir EBG yapısı içerir. 2x2 anten dizisi, dört koaksiyel portun RF sinyalinin fazını ve genliğini değiştirerek -36 ile 36 derece arasında ışın yönlendirme açıları elde edebilir. EBG yapısının dahil edilmesi, genel anten boyutunu %32.2 oranında azaltmıştır, ayrıca antenin kazanç, bant genişliği ve geri dönüş kaybı özelliklerini iyileştirmiştir.

Anahtar Kelimeler: Işın Yönlendirme, Elektromanyetik Bant Boşluklu Yapılar, Yüksek Portlar Arası İzolasyon, Akıllı Antenler, Mikroşerit Anten Dizisi

This thesis is dedicated to my parents

ACKNOWLEDGMENTS

I would like to express my deepest appreciation to my advisor Assoc. Prof. Dr. Tayfun Nesimoglu for overseeing this project, his invaluable contribution, and his profound belief in my abilities throughout the duration of my M.S. program.

I'm extremely grateful to my family who has always nurtured me and never wavered in their support of me.

I would also like to thank Assoc. Prof. Dr. Sedat Görmüş (Karadeniz Technical University, Computer Engineering Department) for for his suggestions and comments.

This study was supported by The Scientific and Technological Research Council of Turkey (TUBITAK), project code: 118E289.

TABLE OF CONTENTS

LIST OF TABLES

TABLES

LIST OF FIGURES

FIGURES

LIST OF ABBREVIATIONS

ABBREVIATIONS	
CSRR	Complementary Split-Ring Resonators
CST	Computer Simulation Technology
DC	Direct Current
EBG	Electromagnetic Bandgap
IBDF	In-Band Full-Duplex
IoT	Internet of Things
ISM	Industrial, Scientific and Medical
LNA	Low Noise Amplifier
MEMS	Micromechanical switches
MPPA	Microstrip Patch Antenna Array
PBG	Photonic Bandgap
RF	Radio Frequency
SAMC	Spiral Artificial Magnetic Conductor
SIC	Self Interference Canceller
SIR	Signal-to-interference Ratio
SNR	Signal-to-Noise Ratio
VSWR	Voltage Standing Wave Ratio

CHAPTER 1

INTRODUCTION

We are witnessing an increased interest towards Wireless Sensor Networks with the introduction of IoT concept. The industrial internet (industry 4.0) applications especially, will be expected to use wireless IoT technologies with the goal of achieving improved efficiency in the next generation automated factory processes. The IoT technologies are expected to enable automation in many aspects of the everyday-life. New business areas will be created based on the value-added applications and services enabled by IoT technology. To enable such value-added applications and services, highly reliable, Internet enabled and low power wireless networks should be created. This has resulted in an increasing demand for smart antenna systems, which have been shown to improve communication system performance in terms of coverage and capacity.

Smart antennas are devices that adapt their radiation pattern in response to changing transmitted or received signals without physically moving the antennas, thus achieving improved performance and efficiency [1]. They are more efficient and more intelligent than conventional antennas in the sense that they allow for the detection of the direction of maximum signal power and steer the antenna beam electronically in the required direction. These systems are becoming popular because of their many benefits. One of the benefits includes increasing the signal-to-interference ratio of the system (SIR). Interference which arises as a result of incoming or outgoing signals from other users unlike noise poses problems as a result of their large amplitude. Since smart antennas work by directing the signal in the direction of a specific user, a large portion of interference is eliminated increasing the SIR. Another major benefit is the added security that is provided especially for governmental, military, and commercial operations that require high-level security,

when a signal is sent in a pre-determined path, it can only be received by a user in that path preventing it from being accessed by the wrong user [2].

Several switchable and steerable beam antennas have been reported over the years, there have been several techniques used to achieve beam steering and switching. The majority of these techniques generally make use of arrays of antennas to alter the direction of the beam [3], [4], some methods utilize switches such as PIN diodes [5], MEMS [6], and varactors [7] to change the characteristics of the antenna to achieve changing patterns while others employ parasitic elements [8]. The phased array antenna is an example of an electronically steerable beam antenna [9] where signals have constructive interference in the desired direction and destructive interference in the unwanted areas. While Phased array antennas are very robust in terms of the precision and accuracy of beam steering, they have a very complex control system and also are very expensive due to the number of phase shifters required.

A simpler and more affordable design uses the Yagi-Uda configuration [10], [11]. A Yagi-Uda antenna also known as a Yagi antenna consists of the main (active) radiating element (driven element or driver) and added coupled elements (parasitic elements) which act as a reflector and one or more directors [12]. When the parasitic element's electrical length exceeds that of the active element, it is referred to as a reflector. and when it is shorter, it is called a director. The reflectors and directors couple together with the active antenna element to alter the radiation pattern. In [13], an antenna design consisting of four microstrip patch antennas arranged around a square patch antenna that acts as the reflector is presented. The design is based on the Yagi-Uda principle which causes the peak of the beam to tilt away from the vertical towards the direction of the directors. Another beam-steering antenna inspired by the Yagi-Uda design is proposed in [14], a multiple-input-multiple-output antenna where the beam reconfigurability is achieved depending on the state of the switch integrated into a metal strip placed between two radiating patches. In [15], a pattern reconfigurable antenna is proposed that can achieve beam steering in seven directions (−60°, −40°, −20°, 0°, 20°, 40°, and 60°). Beam steering is realized

by placing one copper strip on two sides of the square patch antenna, the copper strips have three slits each that is closed or opened using switches making them act as directors or reflectors.

A different approach is to place a parasitic layer above the active antenna element, the mutual coupling of the active layer and parasitic layer induces a current through the parasitic layer, making it possible to alter both radiation pattern and frequency of the antenna [16]. In [17], steering of the main beam in three directions (θ = -30°, 0°, 30°) is achieved using a parasitic 5x5 pixel layer interconnected by 20 switches (PIN diodes). Changing the ON/OFF states of the switches changes the distribution of the surface current of the pixel layer leading to a change in the radiation pattern. This method is usually more efficient because the switches used are isolated from the actively fed element, losses due to switching are very small since they are at a distance from the actively radiating element.

Although designing switchable and steerable beam antennas using microstrip antennas has many benefits which include, low fabrication cost, low profile, and high performance [18], there are also drawbacks. Low gain, narrow bandwidth and relatively big sizes are the major drawbacks of a conventional microstrip antenna [19]. Electromagnetic bandgap (EBG) structures which are a form of metamaterials have been used in literature to overcome these drawbacks. EBG structures eliminates the surface waves produced by the patch antenna thereby improving the overall performance of the antenna. In [20], a simple rectangular microstrip patch antenna built on a Rogers RO3003 with EBG structures at the ground plane is proposed, the introduction of the EBG structure eliminated some of the antenna's surface waves which led to improved return loss antenna, higher bandwidth, and 22.8 % decrease in the size of the antenna compared to the antenna without EBG structure.

Smart antennas are capable of forming radiation patterns which can enable them to receive the desired signal with the maximum power and suppress the unwanted signals significantly. Using such antenna systems can potentially enable energy efficient and high-capacity wireless networks for IoT applications. Also, it is worth noting that majority of the antennas discussed above either have very complex

designs, operate with many switches, or demonstrate low efficiency or gain. The objective of this thesis is to design, simulate and fabricate novel compact switchable beam smart antenna technologies that will be integrated to 6TiSCH networks. The first switchable beam antenna proposed in this thesis is capable of switching its main beam in different directions and also transmitting and receiving signals simultaneously without the use of a circulator due to its high isolation between ports which, to the best of the authors' knowledge, no other reported smart antennas in literature have achieved this. The second smart antenna design uses an EBG ground plane to improve the gain, return loss and bandwidth of the antenna. The size of the antenna is also reduced which is one of the major requirements for IoT applications.

1.1 Objectives

In this research, novel smart antennas are designed. Two types of switchable/steerable beam antennas are investigated with the purpose of obtaining a compact design with improved gain, directivity, and bandwidth. Microstrip antennas are utilized for all the designs because of their lightweight, inexpensive, and compact nature.

The goal of designing the multi-level switchable beam antenna is to develop a dual-port antenna that can change the direction of its radiation pattern and also possess high enough inter-port isolation to reduce the complexity of a full-duplex antenna system. The effects of the Yagi-Uda parasitic layer on a radiating square patch antenna are investigated. The isolation between ports is also studied by comparing the different positions of the ports with their isolation values.

Antenna arrays are typically large and involve a complex control system. Therefore, the objective of designing the 2x2 antenna array is to reduce the overall size of the antenna while improving its performance. To do this, the effects of an EBG structure on the ground plane of the antenna array are investigated by comparing its performance with a conventional antenna array. Beam steering for the second antenna is based on beamforming techniques by changing the amplitude and phase of the RF inputs for each port.

1.2 Thesis Outline

This thesis is organized into five chapters.

Chapter 1 introduces the general topic and summarizes some examples of switchable and steerable antennas presented in the literature. It also explains the objectives of the thesis.

Chapter 2 provides background information on the theory of microstrip patch antennas which covers their characteristics and feeding techniques. EBG structures are introduced and some previous works on EBG structures are reported detailing their benefits. Smart antennas are also discussed, this section explains the different classes of smart antennas, their benefits, and drawbacks.

In Chapter 3, the design, fabrication, and testing of a multi-layered switchable beam antenna with high isolation operating at the ISM band are presented. The beam steering capabilities and the high inter-port isolation property of the antenna are studied. Beam steering is realized by placing a Yagi-Uda parasitic structure consisting of RF switches above a microstrip patch antenna. The antenna has high inter-port isolation to suppress self-interference at the antenna stage.

Chapter 4 presents the design, fabrication, and testing of a 2x2 antenna array with an EBG structure at the ground plane also operating at 2.4 GHz. Beam steering in antenna arrays is achieved by adjusting the phase and amplitude of the input RF signal. The performance of the antenna array with EBG structure on the ground plane compared to that with a conventional ground plane is also studied. The gain and directivity values for different beam steering angles are compared for the antenna with and without EBG.

Chapter 5 presents the conclusion of this thesis along with the future work.

CHAPTER 2

LITERATURE REVIEW

2.1 Microstrip Patch Antennas

An antenna is a component of a transmitting or receiving system that is used to emit or receive electromagnetic waves. It is a type of electrical device that transforms electric power into electromagnetic waves and the other way round from electromagnetic waves to electric power. There are many classes of antennas which include wire, log periodic, aperture, microstrip, reflector, etc.

Microstrip antennas are resonant cavities that are planar and radiate from their edges. It consists of a substrate material with a metal strip on the top and is covered by a ground plane at the bottom. There are many different shapes of microstrip antenna design as shown in Figure 2.1, but the rectangular and square-shaped patch antennas are the most commonly used.

It is one of the most popular classes of antennas due to its low-profile characteristic. In applications such as space, air crafts, and satellites where weight, size, cost, and ease of installation are constraints, low profile antennas such as microstrip antennas are used. It is also used in government and commercial applications with similar restraints and specifications. In addition to being low-profile, microstrip antennas are also simple and cheap to fabricate using modern printed-circuit technology [2]. They are extremely adaptable in terms of resonant frequency, polarization, pattern, and impedance. Reconfigurable pattern, frequency, polarization, and impedance can be achieved by the addition of loads such as pins, varactor diodes, and switches between the ground plane and the patch.

As there are many advantages, microstrip patch antennas also have disadvantages. The basic microstrip patch antenna has a very narrow bandwidth

usually less than 5% (although this is desirable in some applications), low power due to how close the radiating patch is to the ground plane, and high ohmic losses which occur mostly in the substrate and the microstrip feedline [15]. There are methods to improve these characteristics but usually at the detriment of another, for example if the height of the substrate is increased, the efficiency and bandwidth also increases but surface waves that degrade antenna pattern and polarization are introduced.

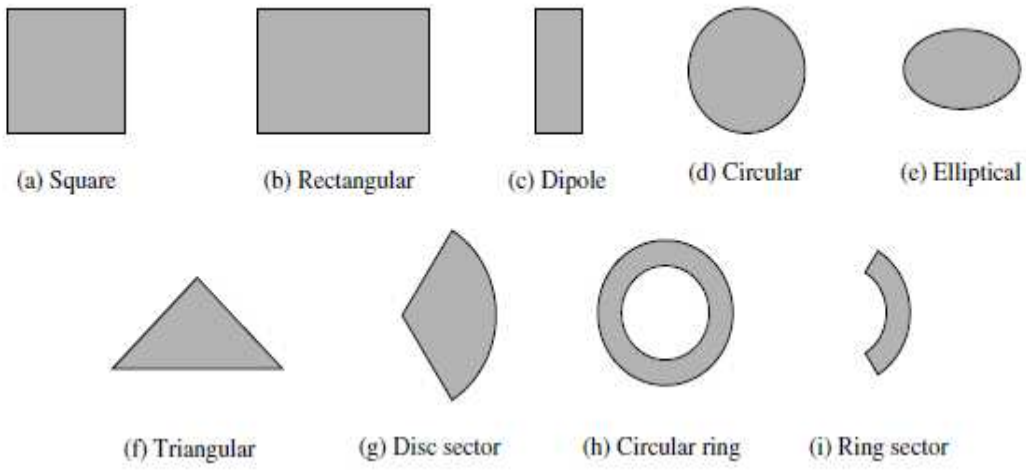

Figure 2.1 Different microstrip antenna geometries

2.1.1 Characteristics of Microstrip Patch Antennas

2.1.1.1 Radiation Pattern

The radiation pattern, also known as the antenna pattern, is a graphical representation of the antenna's radiation properties as a function of space, it details all of the energy radiated into space or received by the antenna [21]. The radiation pattern of an antenna is usually 3-dimensional that is, it radiates in all directions to some degree but it is typically represented with two principal planes (Φ and θ planes) which is obtained by splitting the 3D pattern into two planes (horizontal and vertical) through the maximum point shown in Figure 4.1(a).

Radiation patterns of antennas consist of several types of lobes; a lobe is a section of the radiation pattern surrounded by regions of low intensity of radiation. There are four main types of lobes, the major, back, side, and minor lobes illustrated in Figure 2.2. The major lobe is the most important lobe with maximum power signal and largest beamwidth, the direction of the major lobe shows the directivity. The minor lobes are the unwanted parts of the radiation pattern where energy is wasted, the largest of the minor lobes are the side lobes while the back lobe is in an exactly opposite direction to the major lobe. To improve the efficiency of the antenna these minor lobes have to be eliminated as much as possible to reduce the amount of wasted energy [22]. Radiation patterns have different shapes depending on the type of antenna being investigated. The common types are;

1. Omni-directional pattern
2. Pencil-beam pattern
3. Fan-beam pattern
4. Shaped-beam pattern

The Pencil-beam and Fan-beam patterns are shaped like a pencil and a fan respectively, the Omnidirectional beam is non-directional and has a doughnut-shaped radiation pattern and the Shaped-beam pattern has no uniform shape (pattern-less).

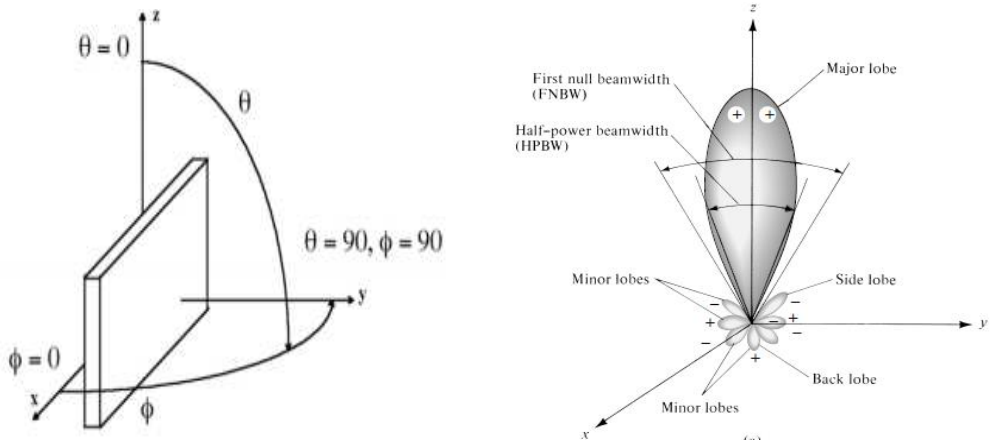

(a) (b)

Figure 2.2 Antenna Radiation Pattern a) Antenna measurement coordinate system, b) Types of radiation lobes

2.1.1.2 Polarization

Polarization of a radiated wave is referred to as "that property of an electromagnetic wave describing the time-varying direction and relative magnitude of the electric-field vector; specifically, the figure traced as a function of time by the extremity of the vector at a fixed location in space, and the sense in which it is traced, as observed along the direction of propagation". There are three polarization types which are linear, elliptical, and circular. The vector describing the time-dependent electric field at a point in space usually traces an elliptical path, this field is described as elliptically polarized. In special cases where the figure traced by the elliptical field becomes straight or circular, the field can be said to be either linear polarized or circular polarized, respectively. A typical time-dependent trace is depicted in Figure 2.3 below.

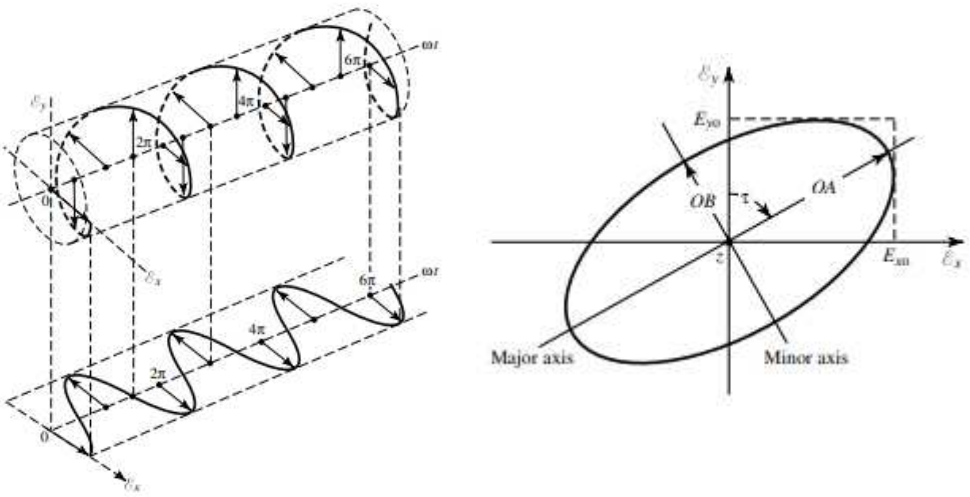

Figure 2.3 As a function of time, the motion of a plane electromagnetic wave as well as its polarization ellipse at z = 0.

The electric field is described as linearly polarized if the vector that describes the field at a point in space and time-dependent is guided along a line. When the electric field is perpendicular to the Earth's surface, the antenna is vertically linear polarized; when the electric field is parallel to the earth's surface, the antenna is horizontally linear polarized. A circularly polarized antenna emits power in all planes in the propagation direction. The propagation plane rotates circularly, achieving one complete cycle in one wave period.

2.1.1.2.1 Co-Polarization and Cross-Polarization

Although there is no universally accepted definition for cross-polarization, it can be explained in terms of a reference or desired polarization also known as co-polarization. Cross-polarization describes any polarization perpendicular to the co-polarization, it refers to transmitting in one polarization state and receiving in the orthogonal polarization state. For linear polarization, if the co-polarization is vertical, then the cross-polarization is horizontal and vice-versa. In the case of circular polarization, if the co-polarization is Right Hand Circularly Polarized

(RHCP), the cross-polarization is Left Hand Circularly Polarized (LHCP) and vice versa.

2.1.1.3 S-Parameters

The scattering matrix of a microwave network is referred to as S-parameters. S-parameters define an electrical framework's input-output relationship between ports (or terminals). For example, if we have 2 ports (Port 1 and Port 2), S12 indicates power transfer from Port 2 to Port 1 while S21 indicates power transfer from Port 1 to Port 2. All in all, SNM represents power transfer from Port M to Port N in a multi-port system.

It is possible to describe a port loosely as any place where we can deliver voltage and current. So, if we have a two-radio communication system (radio 1 and radio 2), then the two ports will be the radio terminals (which deliver power to the two antennas). The reflected power radio 1 attempts to deliver to antenna 1 will then be S11. The reflected power radio 2 attempts to deliver to antenna 2 will be S22. And S12 is the power from radio 2 that is supplied to radio 1 through antenna 1. S-parameters are typically a function of frequency (change with frequency). The S-parameter is usually represented in terms of decibels just like many other antenna parameters, this is to avoid the change in large amounts of quantity when represented in linear magnitude.

$$PdB = 10 \log_{10} P \quad (1)$$

Where,

P = Power in Watts

P dB = Power in decibels

2.1.1.4 Directivity and Gain

Directivity can be defined as "the ratio of the main beam's power density in a given direction to the mean power density over all directions". Directivity property increases with increasing patch size. It does not depend on substrate thickness since the radiation/power intensity and radiated power depends on the thickness, in the same manner, leaving directivity the same, it also is non-dependent on the resonance frequency [23]. In the mathematical form, directivity can be expressed as

$$D = \frac{4\pi U}{P_{rad}} \tag{2}$$

Where,

D = directivity (dimensionless)

U = radiation intensity (W/unit solid angle)

P_{rad} = total radiated power (W)

Antenna gain (in a specific direction) is described as "the ratio of the intensity, in a given direction, to the radiation intensity that would be obtained if the power accepted by the antenna were radiated isotropically. The radiation intensity corresponding to the isotropically radiated power is equal to the power accepted (input) by the antenna divided by 4π" [2]. The gain of an antenna increases as the resonance frequency increases because of the increase in the efficiency of the power radiated [23]. The gain of an antenna system can be represented in the mathematical form given in (3).

$$G = 4\pi \frac{U(\theta, \Phi)}{P_{in}} \tag{3}$$

Where P_{in} is the total input power.

Antenna gain is proportional to both antenna directivity and beamwidth. Higher gain antennas gain additional power by concentrating it on a smaller area (higher directivity); therefore, the higher the gain, the narrower the area covered (measured in degrees of beamwidth). Beamwidth and gain are always inversely proportional.

2.1.1.5 Input Impedance

The input impedance of an antenna is "the impedance presented at its terminals or the ratio of the voltage to current at a pair of terminals or the ratio of the appropriate components of the electric to magnetic fields at a point" [2]. The impedance of the input transmission cable must be matched to the impedance of the antenna to achieve an efficient energy transfer. When the antenna's input impedance is unmatched to the impedance of the input transmission line, there will be antenna system degradation due to input power reflection. Input impedance is usually measured with respect to the transmission line's characteristic impedance [24]. The amount of input voltage (V) reflected can be obtained by first calculating the reflection coefficient (ρ) using (4), then multiplying the reflection coefficient by the input voltage.

$$\rho = \frac{Z_A - Z_0}{Z_A + Z_0} \tag{4}$$

Z_A is the impedance of the antenna and Z_0 is the characteristic impedance. In a system where there are both incident and reflected waves, these waves combine to form standing waves depicted in Figure 2.4 [25]. The voltage standing wave ratio is defined as the ratio of maximum to minimum voltage (VSWR).

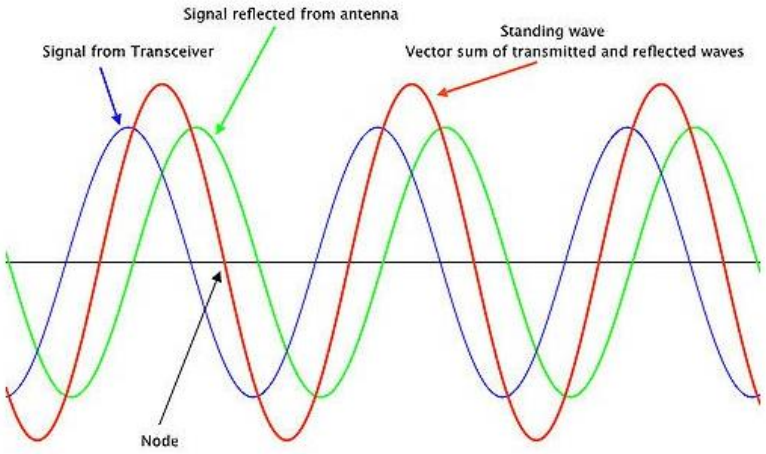

Figure 2.4 Graph showing transmitted and reflected signals forming a standing wave

$$VSWR = \frac{V_{max}}{V_{min}} = \frac{1 + |\rho|}{1 - |\rho|} \quad (5)$$

(5) gives the mathematical representation of the voltage standing wave ratio. Reflection of incident signals causing standing waves does not only reduce the system's efficiency but also introduces distortion to the transmitter which can damage the transmitter. Therefore, it is important to minimize the reflection and the VSWR.

2.1.1.6 Bandwidth

Antenna bandwidth refers to the frequency range over which the antenna's performance in terms of some characteristics adheres to a particular standard. Generally, return loss and VSWR are the characteristics used to define the bandwidth of an antenna [26], [27]. The return loss of an antenna is the measurement of the amount of the antenna's received power from the transmission line. For the antenna to accept all the transmitted power, the antenna's input impedance must perfectly

match the impedance of the transmission line. However, the impedance matching changes with frequency, resulting in a range of frequencies where the amount of return loss is acceptable. The bandwidth is a measure of this acceptable range. The 10 dB return loss bandwidth is the most commonly used measurement for bandwidth where at least 90% of the transmitted power is being received by the antenna [28].

For the design of microstrip antennas, different types of substrates can be used with their dielectric constant ranging from 2.2 to 12. Thicker substrates are usually preferred in terms of antenna performance as they have lower dielectric constants which results in larger bandwidth, higher efficiency and better radiation power. However, the improvement in antenna performance is achieved at the expense of having a larger antenna with increased dielectric loss, weight and surface wave loss. Utilizing a thin substrate on the other hand leads to achieving a smaller antenna with less weight and lower dielectric loss but at the expense of the bandwidth and efficiency. Therefore, designing an antenna requires finding the right balance between the weight, size, efficiency and bandwidth required for the application.

Microstrip antennas have very narrow bandwidths usually less than 5% which is one of the disadvantages of using them. Several methods have been used to improve the bandwidth such as increasing the thickness of the dielectric substrate, using substrates with a lower dielectric constant value, and introducing slots or holes in the patch of the antenna. Bandwidth enhancement is achieved in [29] by etching a rectangular slot on the radiating patch of the antenna. With this technique, an impedance bandwidth of 133% was obtained. A 67% improvement in bandwidth compared to the conventional antenna was presented in [30] by using a ground plane loaded with complementary split-ring resonators (CSRRs). The resonators significantly reduce the guided wavelength of the antenna by exhibiting strong dispersion close to the resonance frequency, this leads to an increase in the bandwidth.

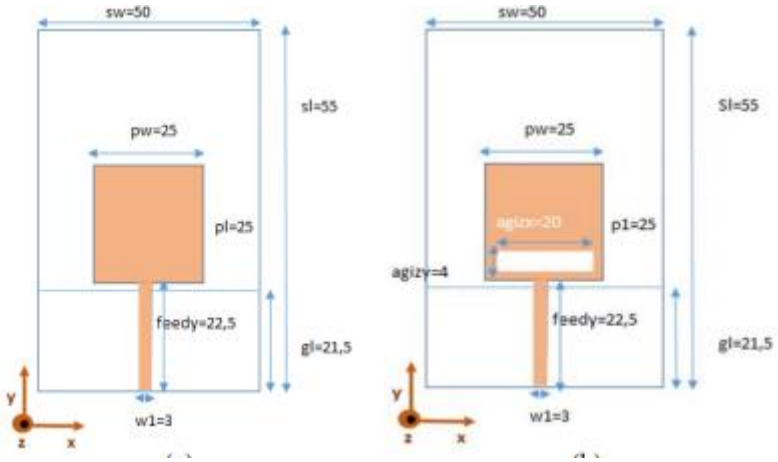

Figure 2.5 Microstrip patch antenna with rectangular slot [29]

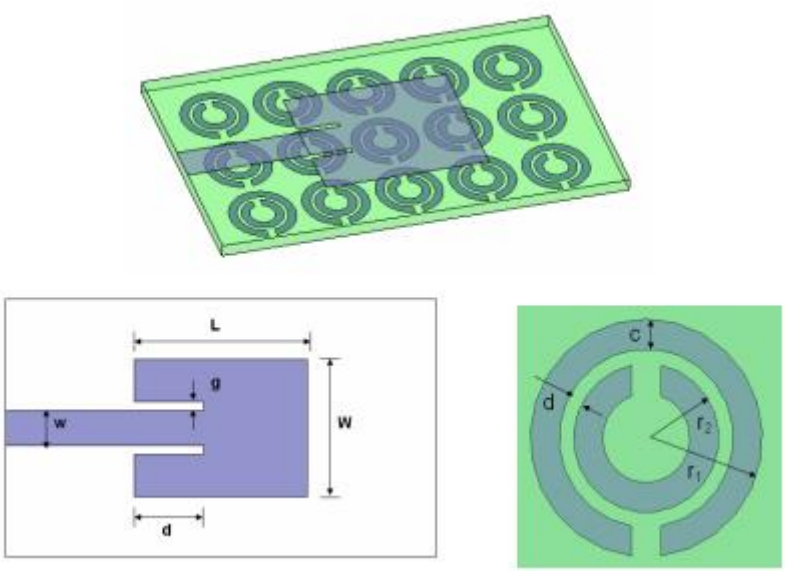

Figure 2.6 Microstrip patch antenna loaded with CSRR [30]

2.1.2 Feeding Techniques

There are many feeding techniques used to design of microstrip antennas. The four most commonly used techniques are coaxial probe, microstrip line, proximity-coupling, and aperture-coupling displayed in Figure 2.7. Both coaxial probe and microstrip line are categorized as contacting while proximity-coupling and aperture-coupling and are non-contacting types of feed.

The microstrip line feeding technique in Figure 2.7(a) involves connecting a conducting strip of metal to the radiating patch, the strip is usually of a smaller width than that of the patch. To achieve good impedance matching and eliminate the need for a matching circuit, an inset cut is made in the patch to fit the conducting strip, the impedance matching will depend on the inset position. This type of feeding has the advantage of making fabrication easy since the same metal and substrate as the rest of the antenna is used. The major disadvantage is that surface wave and spurious feed radiation increases with the thickness of the substrate, this limits the bandwidth of the antenna [31].

The coaxial probe feed shown in Figure 2.7(b) is made up of an inner and outer metal conductor separated by a substrate. The conductor located on the inside is linked to the radiating patch while the conductor on the outer part is connected to the ground. This feeding type is also easy to fabricate and unlike the microstrip, the feedline has low spurious radiation but still faces the problem of very low bandwidth.

The aperture-coupled feeding technique depicted in Figure 2.7(c) employs two substrates isolated by the ground plane, the substrate that is on top separates the patch from the ground, while the feed substrate is placed below the ground. The microstrip feedline is etched on the bottom of the feed substrate whose energy is coupled to the patch through a slot on the ground plane. This technique reduces spurious radiation because of the isolation of the feedline from the radiating patch provided by the ground plane. Some of the setbacks of using the aperture-coupled feeding technique are the required multiple layer fabrication and back lobe radiation increase [15].

Proximity-coupled feed shown in Figure 2.7(d) consists of two substrates, the patch is etched on the top substrate while the microstrip feedline is etched between the top and bottom substrate at a location to obtain good impedance matching, the ground is placed below the bottom substrate. This method of feeding eliminates spurious radiation as there is no contact between the feedline and radiating patch.

The main disadvantage of this method is that it requires multilayer fabrication which increases size.

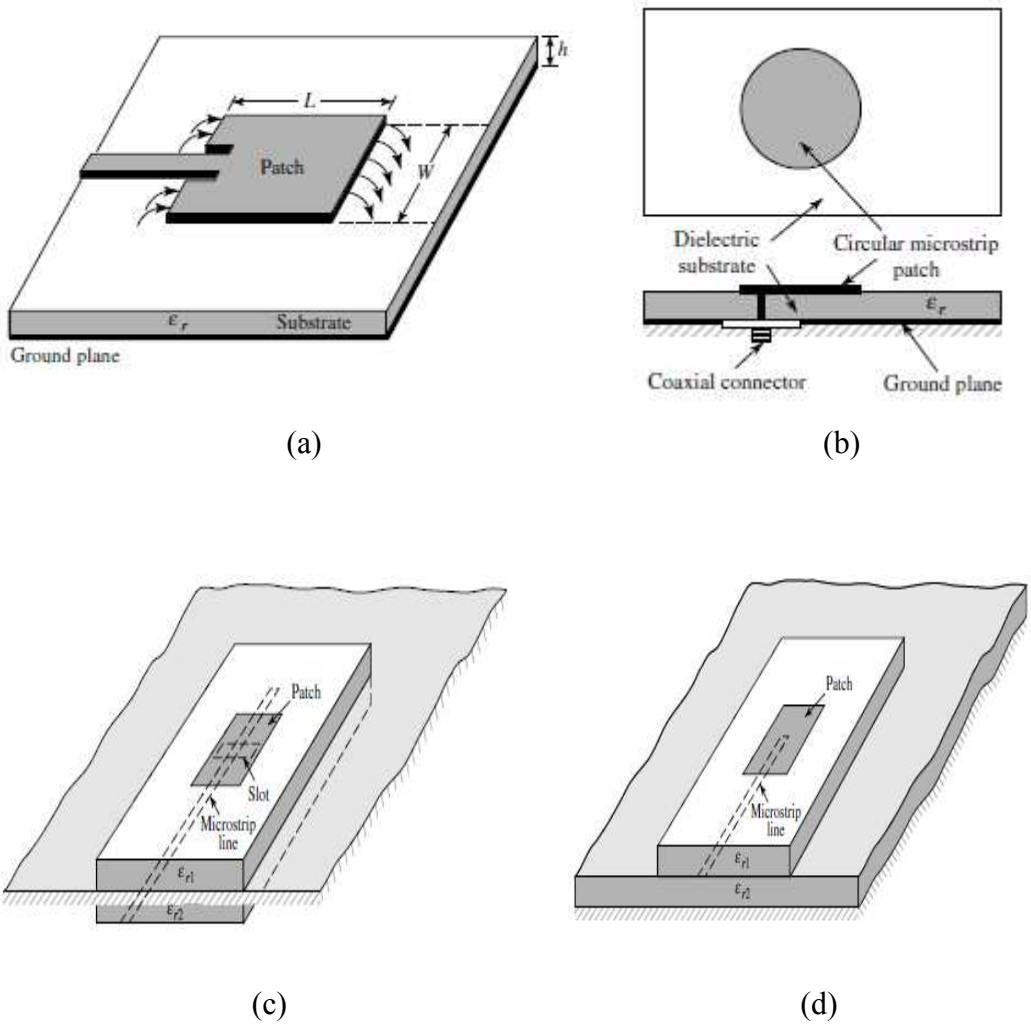

Figure 2.7 Microstrip antenna typical feeding techniques; a) Microstrip line feed, b) Coaxial probe feed, c) Aperture-coupled feed, d) Proximity-coupled feed [32]

2.2 Electromagnetic Bandgap Structures

Electromagnetic band-gap structures can be defined as dielectric or metallic elements arranged in a periodic manner that is capable of blocking electromagnetic

waves in a specific frequency range for all states of polarization and all incident angles [33]–[35]. EBG structures are based on Photonic Bandgap (PBG) structures which were originally photonic crystals with forbidden band-gap for light emissions developed in the year 1987. While PBG is used in the optic domain and solid-state physics, EBG has applications in the microwave domain. EBG structures can be classified as some form of metamaterials because of the special bandgap feature they possess. Metamaterials are artificially created periodic structures that possess characteristics that are not naturally occurring and can manipulate and interact with electromagnetic waves [20]. The bandgap of EBG structures is formed as a result of the interplay between microscopic and macroscopic resonances of the periodic structure.

EBG structures can be incorporated into any part of the antenna such as the ground plane, substrate, or on top of the substrate. Examples of EBG structures designed on top of the substrate can be seen in [36], [37], where mushroom-like EBG cells are placed between antenna elements of an antenna array periodically and linked to the ground via pins through the substrate. Placing the EBG structures at this location prevents the reflection of surface waves incident on the ground from reaching the antenna elements, which resulted in the decrease in mutual coupling between the antenna array. A pinwheel-shaped slots EBG substrate used for dual-band patch antenna shown in Figure 2.8 is presented in [38] where the EBG structure is integrated into the substrate of the antenna. The EBG substrate used in this paper is an improved version of the traditional mushroom-like EBG substrate. The proposed design addressed smaller frequency drifts better resulting in improved gain, bandwidth, and radiation efficiency. In [39], four 2x2 microstrip patch antenna arrays (MPAA) with four different variations of the spiral artificial magnetic conductor (SAMC) based ground plane are compared with a conventional 2x2 MPAA with no modifications to its ground plane. The concept of the spiral ground plane is similar to that of the spiral antenna therefore, it can be categorized as a broadband structure. As a result of this, the antenna bandwidth was found to be extended from 0.5 GHz to 20 GHz and the gain increased from 6.5 to 10.5 dBi.

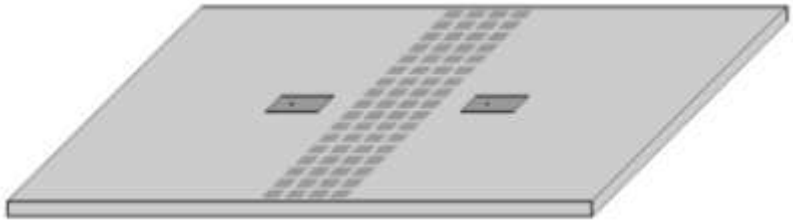

Figure 2. Mushroom-like EBG structure placed between the patch antennas for a low mutual coupling [37]

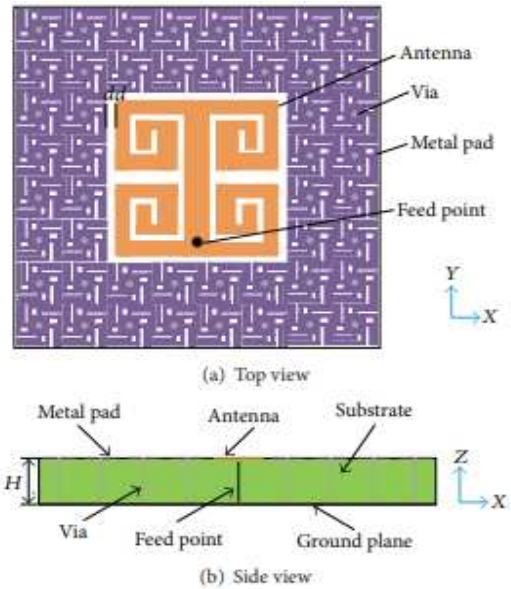

Figure 2.8 A spiral slot patch antenna is configured with an EBG substrate. [38]

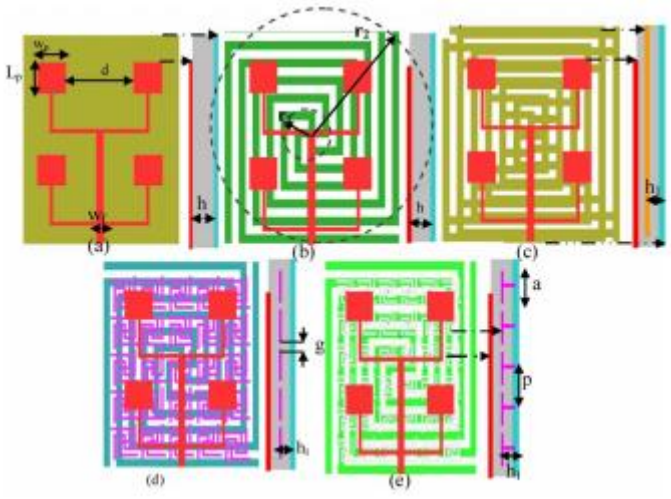

Figure 2.9 Different prototype geometries of 2x2 microstrip patch antenna arrays with different EBG configurations [39]

EBG structures have been widely used in microwave systems especially antennas to suppress surface waves. Surface waves of a microstrip antenna are waves that are excited when the relative permittivity of the substrate is greater than 1. They are generated when the incident wave passes through the interface between two dissimilar mediums, some of the incident waves are transmitted while the rest is reflected. The excitation of this wave results in multiple reflections throughout the length of the antenna between the ground and substrate. Surface waves once formed, are trapped and continuously propagate within the interface where they are generated until they reach discontinuities such as the edge of the material and then diffract into the surrounding. The radiated wave at the discontinuities shown in Figure 2.11 forms a ripple pattern that in turn interferes with the antenna's main radiation with any circuit or antenna element around it thereby resulting in losses [40].

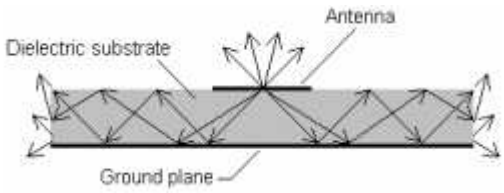

Figure 2.10 Surface wave propagation inside the grounded dielectric slab [41]

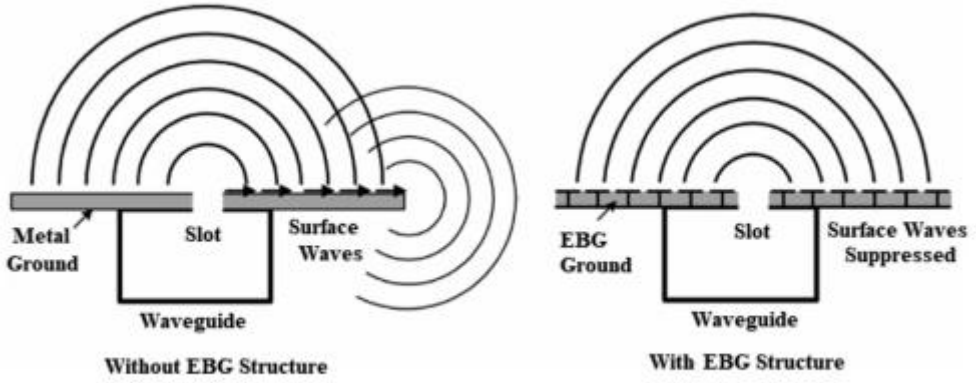

Figure 2.11 The suppression of unwanted surface waves by EBG structure [42]

2.3 Smart Antennas

A smart antenna system is a system consisting of several antennas, corresponding RF hardware and, a digital signal processor to control the direction of the signal. In truth, antennas alone are not smart, it is the entire system that is smart. Smart antennas fall under two major categories which are switched beam smart antenna and adaptively beam steering smart antenna [43] as shown in Figure 2.12.

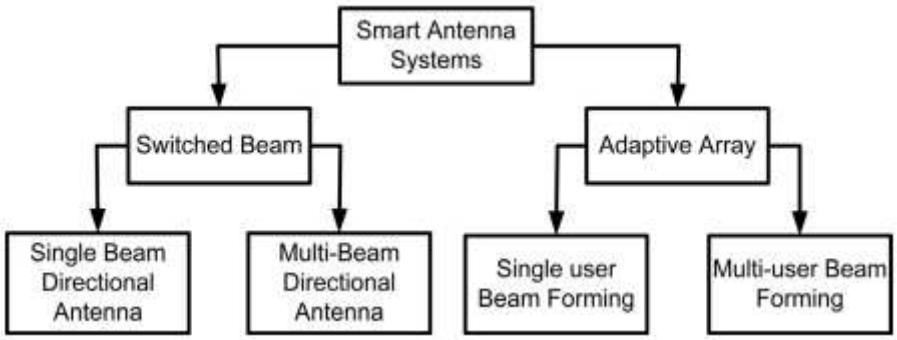

Figure 2.12 Classification of Smart Antenna Systems

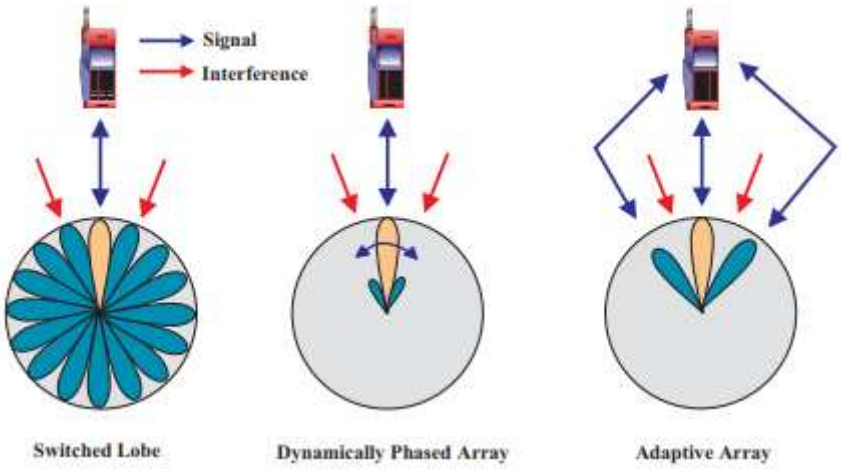

Figure 2.13 The working mechanism of the switched beam, dynamically phased array, and adaptive array smart antenna systems [44]

2.3.1 Switched Beam Smart Antenna System

In terms of complexity and cost, the switched beam smart antenna system is the most basic type of smart antenna. The system generates a predetermined number of beams with increased sensitivity in predetermined directions [45]. It can detect signal strength in all directions and choose one of the beams based on a set of criteria [44].

2.3.2 Phased array or multi-beam antenna

Phased array or multi-beam antennas refer to antennas with a single beam that can steer towards one desired direction or a set of pre-defined beams where one beam is selected towards the required direction. Phased array antennas are similar to switched beam antennas except for having a better intra-cell handoff. Intra-cell handoff refers to the transfer of a user from one range of beam to another as they move away from the perimeter of the beam. The better intra-cell handoff is a result of the direction of arrival (DoA) algorithm that tracks the user's signal.

2.3.3 Adaptive Array

This type of smart antenna system has by far the highest level of performance to date. It is an array of multiple antenna elements with a state-of-the-art signal processing algorithm. As the name suggests, the system is capable of adapting the antenna pattern to environmental changes to improve the signal-to-noise ratio (SNR) of the desired signal. Each antenna element is weighted with the weight being updated frequently to achieve maximum gain in one direction while trying to minimize gain in another.

2.3.4 Advantages of Smart Antenna Systems

A. Capacity Increase: Mobile systems in locations with high population are typically interference-limited, which means that the primary source of noise in the system is interference from other users. As a result, the signal-to-interference ratio (SIR) is much lower than the signal-to-noise ratio (SNR). Smart antennas generally improve the SIR by increasing the level of the valuable received signal and decreasing the level of the interference simultaneously.
B. Increased Range: Since smart antennas are directional in comparison to sectorized and omnidirectional antennas, there is potential for increased range [27]. In other words, smart antennas can direct their power toward the potential recipient rather than wasting it in other directions where they are not needed, as omnidirectional antennas do [46].
C. Increased Security: Security is an important issue in a society that is increasingly reliant on the internet for business operations and personal information transmission. Smart antennas make tapping a connection more difficult since for the intruder to tap a connection successfully, they have to be positioned in the same path as the user as seen from the base station.
D. It may also increase the power efficiency of a Tx-Rx chain because instead of using an isotropic antenna (0 dB gain), a higher gain antenna may be used that can be steered in the required direction.

2.3.5 Drawbacks of Smart Antenna Systems

A. Complex: Smart antennas have the disadvantage of being far more complicated than traditional antennas[46]. This means that faults or problems may be more difficult to detect and more likely to occur.
B. Larger Size: Smart antenna systems are significantly larger than traditional systems due to the antenna arrays that are used. Antennas can be aesthetically unappealing or unsightly in social situations, which might be a problem.

C. Expensive: Smart antennas are far more expensive than traditional antennas because they are extremely complex and use cutting-edge processing technology.

2.4 Self-Interference Elimination in Full-Duplex Antenna Systems

Full-duplex antennas conventionally refer to antennas that can transmit and receive signals at the same time using two separate carrier frequencies to eliminate the effects of self-interference. Self-interference is simply described as the leaked signals from a transmitter to a receiver. It is the biggest challenge that has to be overcome in any full-duplex antenna system [47]. Many smart antennas that have been designed in the past rely on frequency division, time division, or the use of circulators for signal transmission which usually makes the transceiver design much more complicated. This is largely due to the long-standing assumption that full-duplex communication cannot be realized by using a single antenna at the same frequency band, at least two antennas need to be utilized [48], [49]. This assumption was made because of the self-interference that is produced in the antenna system during the communication process.

Half-duplex schemes which consist of Time division duplex and frequency division duplex are no longer viable in a world where an increasing number of applications demand bandwidth from a finite electromagnetic spectrum [50]. Because of this, many researchers have attempted to debunk this assumption. When compared to traditional multiplexed schemes, in-band full-duplex nearly doubles spectral efficiency. Recently the term has been extended to cover antennas that can simultaneously communicate in two directions while operating on the same carrier frequency [51].

Several techniques have been used in literature to achieve self-interference cancellation, some of these techniques include antenna separation, analog, and digital cancellation techniques [52]. Self-interference elimination is usually carried

out in four stages of the In-Band Full-Duplex (IBFD) transceiver shown in Figure 2.14 [53]:

A. Antenna cancellation
B. RF cancellation
C. Analog cancellation
D. Digital base-band cancellation

Antenna cancellation usually employs methods to reduce the mutual coupling that is inherent between the transmit and receive ports of the antenna and then utilizing external circuitry to increase the isolation. Paper [53] presents a dual-port orthogonal polarized square patch antenna that was able to provide about 45 dB inter-port isolation due to cross-polarization of the ports. To increase the isolation, an external feed-forward loop consisting of voltage variable phase shifters and a digital step attenuator was implemented between the transmit and receive ports. This external circuitry increased the isolation from 45 dB to 66.1 dB.

RF cancellation which is done prior to signal transmission involves sampling or tapping a portion of the transmitted signal. Following that, adjustments are made to the gain and delay using a finite impulse response (FIR) filter to cancel out the coupling of the receiver into the transmitter [54]. The design for the second and third stages of self-interference cancellation was presented in [54]. In this paper, a finite impulse response filter acts as the RF self-interference canceller (RF-SIC) and is connected along the transmit chain between the power amplifier (PA) and the low noise amplifier (LNA). This filter allows the received signal transferred by the LNA into the receiver to be devoid of transmitted signal noise and non-linearities involved. Frequency retranslation technique presented in [55] is also used for interference suppression. This signal cancellation process behaves like a sharp band-stop filter with a high stop-band attenuation that suppresses the wanted signal from the input signal to obtain the error signal. The input of the receiver is then pre-distorted with the error signal so as to receive the wanted signal without interference.

Analog cancellation is very similar to the RF cancellation except for the fact that it is done after the reception of the transmitted signal to get rid of any residual noise from the received signal.

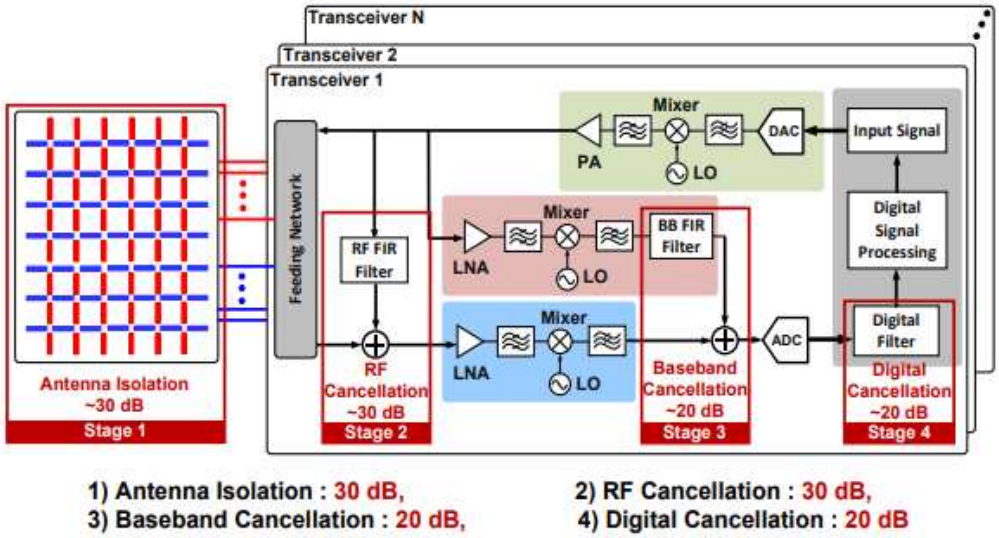

Figure 2.14 A simultaneous transmit and receive system showing the different cancellation stages

The digital base-band cancellation is implemented after receiving and converting the signal from analog to digital. The goal of digital cancellation is to reduce self-interference power below the noise floor [50].

CHAPTER 3

A MULTI-LAYERED SWITCHABLE BEAM SMART ANTENNA

A switchable beam antenna is the simplest type of smart antenna that consists of two or more antennas. It has a fixed radiation pattern with a fixed number of beams which is dependent on the number and arrangement of the elements of an antenna. It works by switching to one or more beams in the direction of the strongest signal power to enhance performance and maximize efficiency. The multi-layered switchable beam smart antenna combines the concept of the Yagi-Uda antenna for beam steering and orthogonal polarization to achieve high inter-port isolation for SI elimination.

3.1 Square Patch Antenna Design

For the design of the multi-layered switchable beam smart antenna, the square-shaped patch antenna shown in Figure 3.1 is used as the bottom layer. The individual patch antenna is designed using copper for the ground plate and the patch, (which includes the feedline) both with a thickness of 0.035 mm and Rogers RO4003C is used as the substrate, the Rogers substrate has a thickness of 0.8 mm and a relative dielectric constant of 3.38. Copper, Silver, and gold are the major materials used for microstrip ground and line, copper is commonly used because it is the hardest and cheapest of the three. Rogers RO4003C substrate is utilized because of its low dielectric and electrical signal losses, better thermal management characteristics compared to FR-4, and its excellent high-frequency performance. The feeding technique used is the coaxial probe shown in Figure 2.7(a). Impedance matching is achieved by adjusting and optimizing the position of the RF ports [31]. For a square patch antenna, the width (W) is calculated first and then used to obtain the length (L). The width is assumed to be equal to the length for a square patch

antenna as seen in Table 3.1, then the design is optimized to operate at the desired frequency.

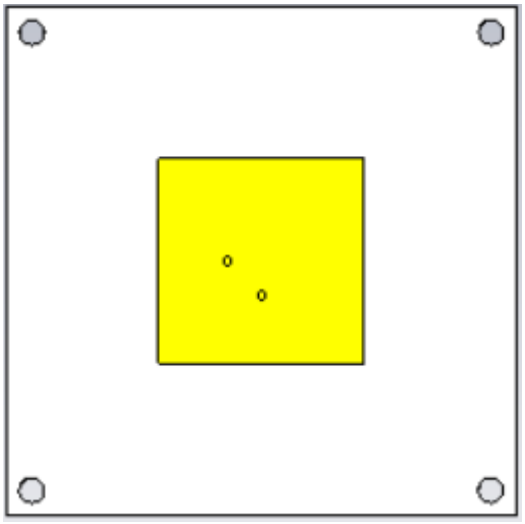

Figure 3.1 Square patch antenna

To design the square patch antenna, the following formulas are used to obtain the dimensions [19], [20];

$$W = \frac{c}{2f\sqrt{\frac{(\varepsilon_r + 1)}{2}}} \tag{6}$$

$$\varepsilon_{reff} = \frac{\varepsilon_r + 1}{2} + \frac{\varepsilon_r - 1}{2}\left[1 + 12\frac{h}{W}\right]^{\frac{1}{2}} \tag{7}$$

$$\Delta L = 0.142\frac{\left(\frac{W}{h} + 0.264\right)(\varepsilon_{reff} + 0.3)}{(\varepsilon_{reff} - 0.258)(\frac{W}{h} + 0.8)} \tag{8}$$

$$L = \frac{c}{2fr\sqrt{\varepsilon_{reff}}} - (2 \times \Delta L) \tag{9}$$

$$\lambda = \frac{c}{f} \tag{10}$$

$$\lambda_g = \frac{c}{f\sqrt{\varepsilon_{reff}}} \tag{11}$$

Where

c velocity of light in air (m/s^2)

f Resonance frequency (Hz)

h height of the substrate (mm)

ε_r relative dielectric constant

ε_{reff} effective relative dielectric constant

λ wavelength (mm)

λ_g guided wavelength (mm)

3.2 A Multi-Layered Switchable Beam Smart Antenna

The proposed antenna is a square microstrip patch antenna with a parasitic layer working at the 2.4 GHz ISM band, the parasitic layer has Yagi-Uda antenna properties (with the reflectors and directors located around the driven element) and is controlled by inserting switches between the copper strips serving as the reflectors and directors. Changing the states of the switches either lengthen or shorten these copper strips bringing about the steering of the main beam to one of the four sides of the square patch antenna at an angle depending on the state of these switches. Work similar to this is presented in [15].

The dimensions of the bottom layer shown in Figure 3.2 were calculated using (6) - (11). It is made up of a 32.5 x 32.5 mm^2 square patch antenna on an 80 x 80 mm^2 Rogers RO4003C substrate of thickness 0.81 mm (a thin substrate is utilized to reduce the attenuation of the main radiation thus improving gain) and relative

permittivity of 3.38. The ground plane directly below the substrate has the same area dimension as the substrate. The bottom layer of the multi-layered switchable beam antenna has two RF ports. To match the impedance of the transmission line to the impedance of the antenna, the first antenna port is placed at a distance away from the center of the patch, this position is usually not symmetrical with the shape, therefore beam steering is only achieved for two sides. Introducing a second coaxial feedline makes it possible to steer in the other two directions thereby achieving a 360° beam steering (in all four sides of the square patch antenna) in the azimuth plane.

The top (parasitic) layer shown in Figure 3.3 and Figure 3.4 consists of copper (0.0175 mm thick) strips placed on the same type and size of Rogers RO4003C substrate used for the bottom layer; its function is to steer the main lobe to the wanted directions. The reflectors and directors are arranged so that they can behave as either directors or reflectors depending on if the switch (PIN-diode) is ON or OFF. Additional lengths of copper strips are added in front of every reflector/director without switches to serve as extra directors to increase the gain of the antenna. This is due to fact that directors receive and retransmit signals from the driver at different phases depending on their length. These signals superpose constructively to enhance the signal properties. The substrate thickness of the top layer is chosen as 0.81 mm to reduce the attenuation of the main radiation thus improving the gain. The air medium separating the top and bottom layers has a dielectric constant of 1 to mimic real-life air medium behavior. The height of the air-gap which is equal to 9 mm was found through optimization to give the best gain and return loss results as shown in the graph of Figure 3.5.

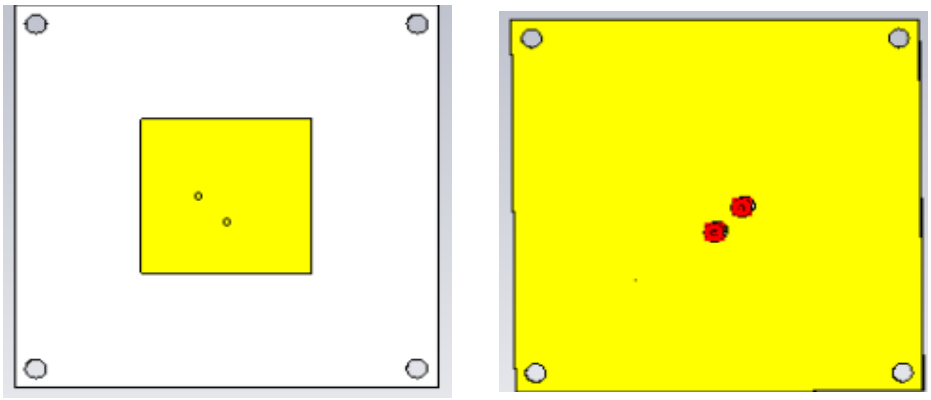

(a) (b)

Figure 3.2 The bottom layer of the multi-layered switchable beam antenna (a) top view and (b) bottom view

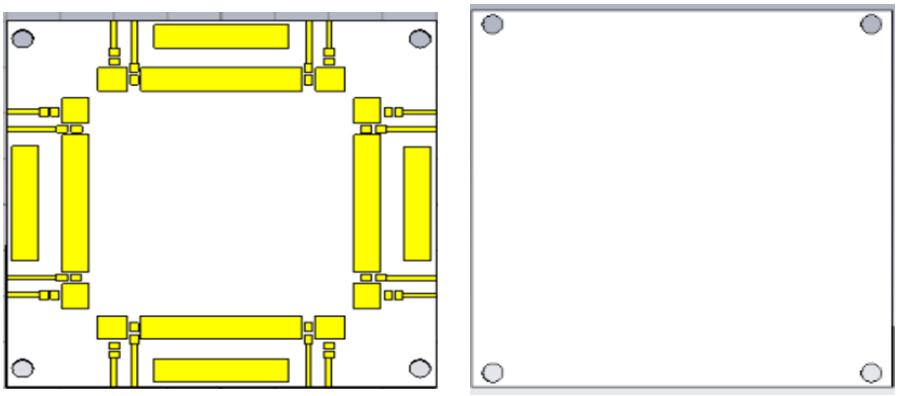

(a) (b)

Figure 3.3 The top layer of the multi-layered switchable beam antenna (a) top view and (b) bottom view

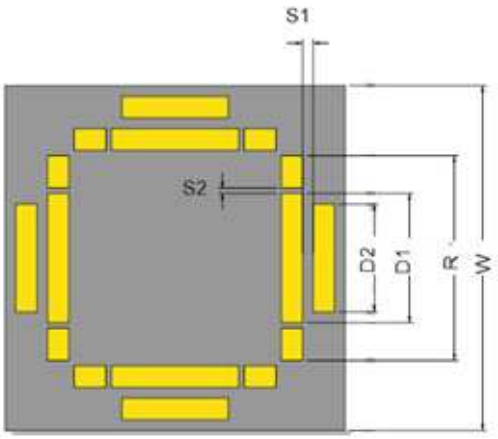

Figure 3.4 Proposed antenna showing the parasitic layer dimensions

Inserting the known values into (6) –(11), the unknown parameters are calculated below;

$$W = \frac{3x10^8}{2 \times 2.4 \times 10^9 \sqrt{\frac{(3.38 + 1)}{2}}} = 42.23\, mm$$

$$\varepsilon_{reff} = \frac{3.38 + 1}{2} + \frac{3.38 - 1}{2}\left[1 + 12\frac{0.81}{42.23}\right]^{-\frac{1}{2}} = 3.26$$

$$\Delta L = 0.142\frac{\left(\frac{42.23}{0.81} + 0.264\right)(3.26 + 0.3)}{(3.26 - 0.258)(\frac{42.23}{0.81} + 0.8)} = 0.1667\, mm$$

$$L = \frac{3x10^8}{2 \times 2.4 \times 10^9\sqrt{3.26}} - (2 \times 0.1667) = 34.28\, mm$$

$$\lambda_g = \frac{3 \times 10^8}{2.4 \times 10^9\sqrt{3.26}} = 69.23\, mm$$

$$Length\ of\ Reflector = 0.55 \times \lambda = 38.08\, mm$$

$$Length\ of\ Director = 0.45 \times \lambda = 31.15\, mm$$

Driven length = 32.50 mm (square patch antenna with coaxial feed)

λ = 70 mm

Director length = 30 mm

Reflector length = 46 mm

Distance between elements ~= λ/10 = 7 mm

Table 3.1 Optimized Antenna Parameters

Parameters	Values
Length (width) of the ground plane (W)	80 mm
Length (width) of the patch	32.5 mm
Height of the air medium	9 mm
Reflector length (R)	46 mm
Director 1 length (D1)	30 mm
Director 1 length (D2)	25 mm

Table 3.2 Properties of the multi-layered switchable beam antenna

Groups	**Layers**	**Material (dielectric constant)**	**Height (mm)**
1	Ground	Copper	ht = 0.0175
	Substrate 1	Rogers RO4003C (3.38)	hs1 = 0.81
	Metallic patch	Copper	ht
2	Substrate 2	Rogers RO4003C (3.38)	hs2 = 0.81
	Reflectors and directors	Copper	ht

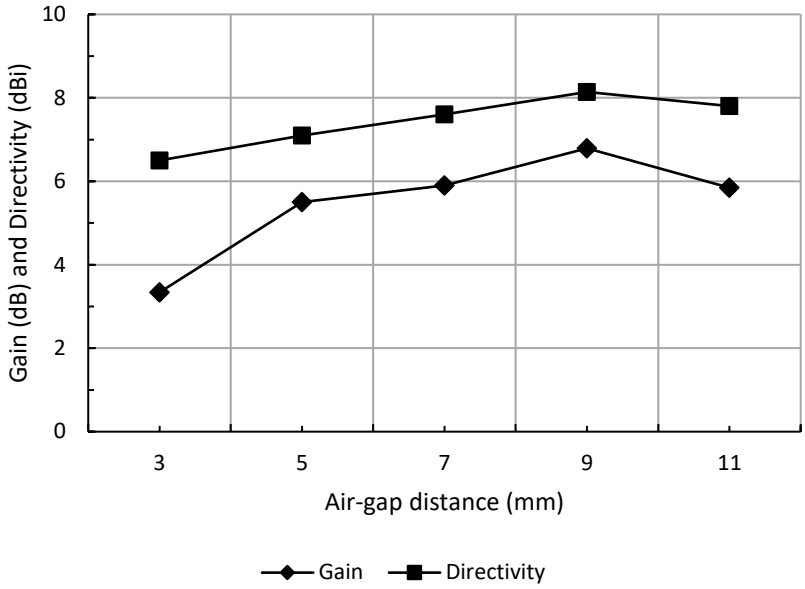

Figure 3.5 A graph showing the gain and directivity values of different air-gap distance

3.2.1 Switching Mechanism

The switches are modeled as the PIN diode equivalent RLC circuit shown in Figure 3.6 during the simulation. The PIN diode used for the antenna design is the SMP1345-040LF PIN-diode. This specific PIN diode is used because of its low capacitance and resistance values, this guarantees that the switches will introduce very low insertion loss in the antenna. The switch acts as a current-controlled variable resistor depending on the bias voltage applied. When it is forward biased, it can be represented with an inductor L, and low resistance R_S connected in series while the reverse biased condition is represented by a parallel combination of large resistance R_P and diode capacitance C_T in series with L. SMP1345-040LF switch has a low series inductance of L = 0.45 nH for both ON and OFF states. For the ON state, R_S = 1.5 Ω and for the OFF state, C_T is typically 0.20 pF while R_P = 2.5 kΩ. All the

switches have two biasing lines per switch, one for supplying DC forward and reverse bias voltage and the other connects the switch to the ground.

The biasing lines for the PIN-diodes are shown in Figure 3.7. DC blocks and RF chokes are used along the biasing lines to block the interference of the RF signal and DC (supply) signals while the bias resistors are used to control the input DC current. 150 pF capacitors are used as DC blocks while inductors of 36 nH and 33 nH are used as RF chokes for the dc voltage and the ground respectively. A large resistance value of 1.5 kΩ is used as the biasing resistor.

Only one of the ports is being supplied at a time depending on the steering direction desired. When the RF signal is supplied through port 1, the beam can be steered in either +x ($\varphi = 0°$) or -x ($\varphi = 180°$) directions by changing the states of switches in the same direction. The opposite applies to port 2, when the RF signal is supplied through port 2, beam steering is possible between +y ($\varphi = 90°$) and -y ($\varphi = 270°$) directions depending on the states of the switches. In the case where RF is supplied to either port 1 or port 2 and all the switches are in the OFF state, there will be no beam steering in any direction. Beam steering for this design is accomplished by changing the surface current distribution of the parasitic layer. Therefore, eight switches that work in pairs along with the two feeding ports are placed between copper strips to lengthen or shorten them when in the ON or OFF states respectively.

In Figure 3.8, when port 1 is supplying RF signal, switches 5 and 6 are ON and the other switches are OFF, the electrical length of the copper strip increases making the surface current denser in this region compared to others. This process causes the main beam to steer towards -x direction. The mode of operation for the other switches is shown in Table 3.3.

Table 3.3 Mode of operation of the switches

Excitation port	**SW 1&2**	**SW 3&4**	**SW 5&6**	**SW 7&8**	**Direction of radiation**

1	ON	OFF	OFF	OFF	+x
1	OFF	OFF	ON	OFF	-x
2	OFF	OFF	ON	OFF	-y
2	OFF	OFF	OFF	ON	+y
1 or 2	OFF	OFF	OFF	OFF	No steering

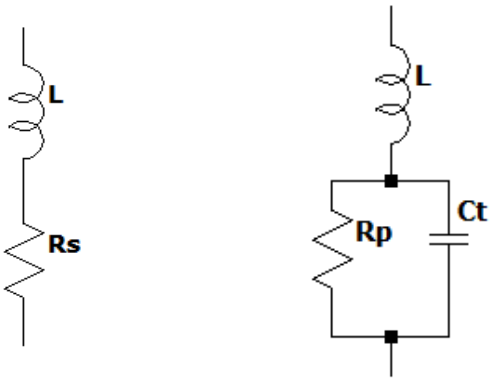

(a) (b)

Figure 3.6 PIN-diode equivalent circuit (a) ON state, (b) OFF state

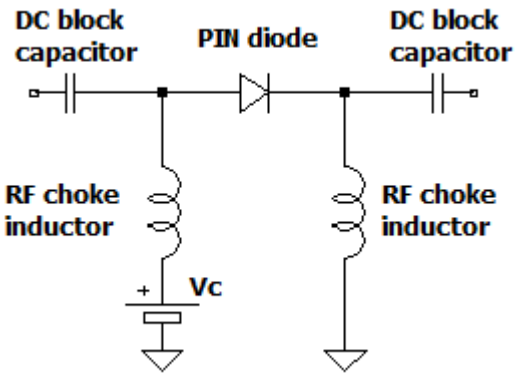

Figure 3.7 PIN diode bias circuit

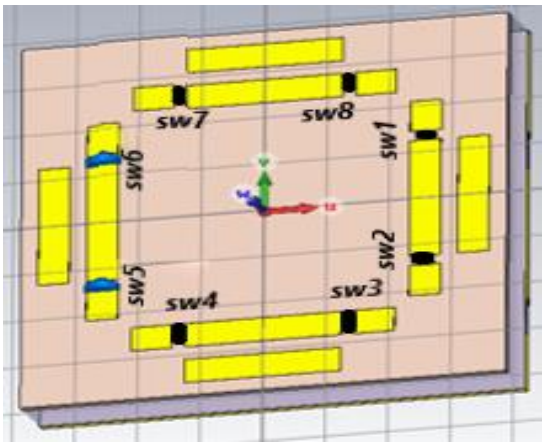

Figure 3.8 Top and bottom layers of the multi-layered switchable beam antenna showing the eight switches

3.2.2 Numerical Analysis

The main objectives for the design of this smart antenna are to demonstrate the steering of its main beam both in the azimuth and elevation planes and to show the high inter-port isolation. The proposed antenna was first simulated and optimized using the time domain solver in CST Microwave Studio. The time domain solver is based on the finite integration technique (FIT) describing Maxwell's equations in a time-grid space. This solver is preferred for the design because it is more suitable for calculations over a wide frequency range compared to the frequency domain solver. The FIT differential method is employed because of some of its advantages over some of the other existing methods such as the finite element method (FEM). When compared to the FEM method, FIT has a simpler algorithm and allows for easy and efficient implementation. Another significant advantage of the FIT method is that it implements parallel computing. Parallel computing is a process where Message Passing Interface pallelization is used to divide the simulation domain into smaller domains with equal sizes, these sub-domains are then sent to parallel computers where EMF simulations are carried out at the same time, thereby reducing total computational time [56]. The finite difference time domain method (FDTD) and FIT

methods have similar advantages and disadvantages and their simulation results have been found to be very close.

The simulation is performed on a port-by-port basis by the time domain solver, which employs a hexahedral or hexahedral transmission-line matrix (TLM) meshing technique. The hexahedral technique uses ten mesh cells per wavelength for the simulation. This number of mesh cells per wavelength is sufficient for this antenna design as increasing the number of cells increases simulation time without significantly improving the simulation results.

The optimization algorithm employed for the antenna design is called the Trust Region Framework (TRM). TRM is a crucial numerical optimization method for solving nonlinear programming (NLP) problems. It functions by first defining a region (also known as the trust region) around the current best solution where a specific model (typically a quadratic model) can estimate the initial objective function to some extent. After this, it takes a step forward based on the region specified. If there is a significant improvement after the step forward, the model is thought to be a good depiction of the initial objective function. If there is a negative or no significant improvement, then the model is not regarded as a good depiction of the initial objective function The convergence can be guaranteed by making the size of the "trust region" in every iteration dependent on the previous improvement.

A simple square patch antenna with two feed points was modeled and simulated to generate the broadside beam that will be steered in different directions. The return loss characteristic of the antenna was obtained and improved by optimizing the position of the feeding ports. After this, the parasitic layer shown in Figure 3.4 was designed in CST and placed above the square patch antenna. To verify the analytical design, the antenna was initially simulated using large resistors around 10 kΩ to represent the OFF switch-state and 1 Ω for the ON state. A more complex biasing circuit was then designed to include the switch states' exact PIN diode equivalent circuit.

The simulated S-parameter result of the two-port system is demonstrated in Figure 3.9 where S11 represents the return loss experienced in port 1 when the beam is in the end-fire direction (no steering) and S22 represents the return loss experienced in port 2 when the beam is being steered. S12 and S21 are the amount of power transmitted from ports 2 to 1 and ports 1 to 2 respectively (isolation between the ports). The high inter-port isolation shown in Figure 3.9 to be around 46 dB is achieved by the orthogonal polarization of the antenna (where the antenna is vertically and horizontally polarized). This means there will be little or almost no power transmitted between the two ports. In theory, orthogonal signals do not interfere with each other since the energy fed into one of the ports does not couple to the second port. Both S11 and S22 are below -20 dB which implies that less than 0.3% of the input power is lost.

The radiation patterns showing beam steering in the elevation and azimuth planes were also observed during the simulation process. The beam can be steered in four directions in the azimuth plane (0°, 90°, 180°, 270°) and can be steered between 0° and 27° in the elevation plane. Figure 3.10 and Figure 3.11 depict the simulated radiation pattern of the multi-layered switched beam antenna.

In Figure 3.10(a), the switches on the right side are on, therefore steering the beam in the right direction (+y), when all switches are OFF, the beam is not steered in any direction as seen in Figure 3.10(b), Figure 3.10(c) shows the beam steering in -y direction. The beam is steered at an angle of 27° for all four directions with a gain of 6.19 dB and directivity of 7.75 dBi, for the broadside direction when all the switches are OFF, the gain is 6.28 dB and directivity is 7.71 dBi. The surface current distribution further explains the beam steering mechanism as illustrated in Figure 3.12. When all the switches are OFF, the surface current on the metal strips (directors/reflectors) is less dense as shown in (a) because they are not connected compared to (b), where one of the pairs of PIN-diodes is turned ON, the metal strips are connected and there is more surface current moving through.

Table 3.4 provides the gain and directivity values for the proposed antenna when the beam is steered in any direction and when there is no steering (φ = 0°, Θ = 0°). High gain, directivity, and efficiency values were obtained during the simulation for all the cases.

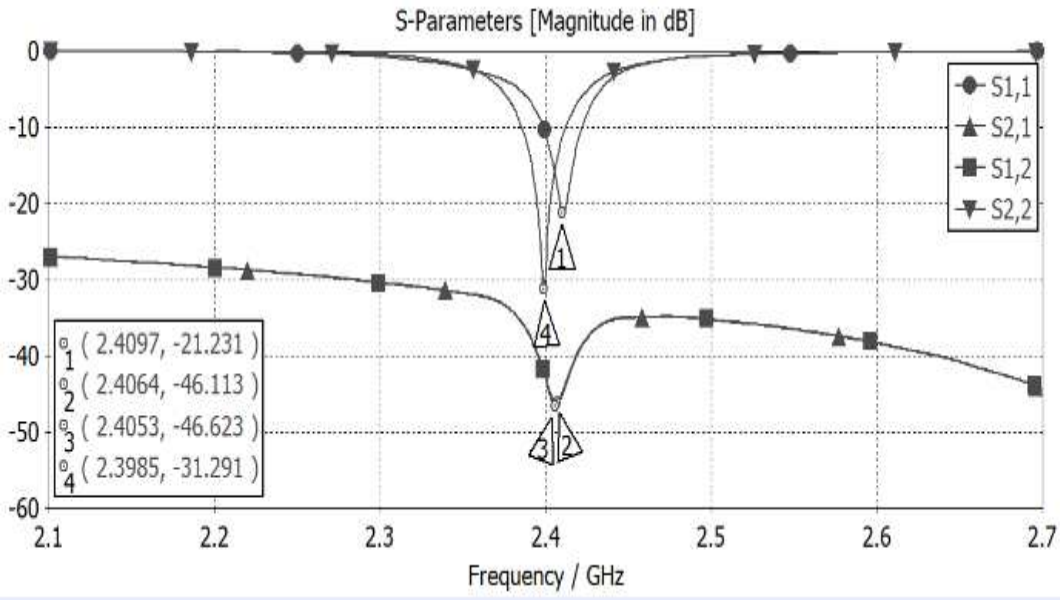

Figure 3.9 S-parameter graph of the Multi-Layered Switchable beam antenna where S11 = -21.231 dB, S22 = -31.291 dB, S12 = -46.113, S21 = -46.623 dB

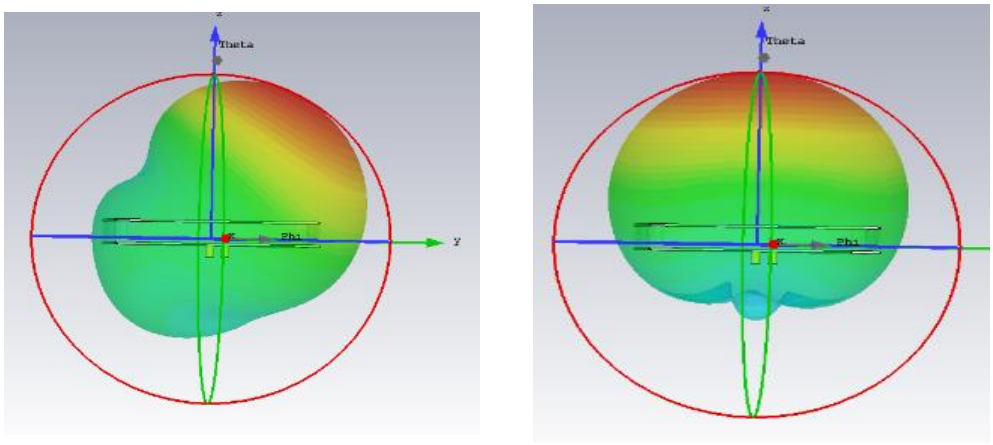

(a) (b)

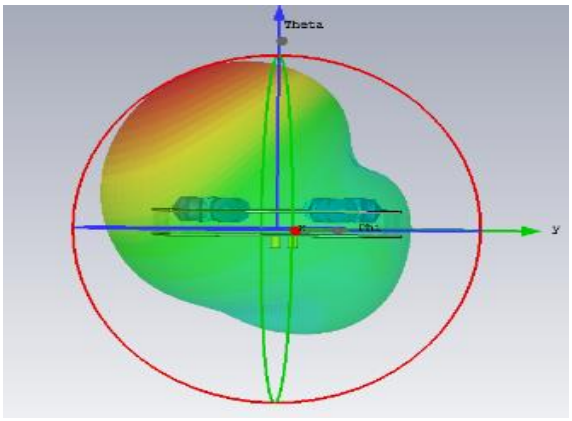

(c)

Figure 3.10 Far-field pattern for elevation plane steering (a) 27°, (b) 0°, (c) -27°

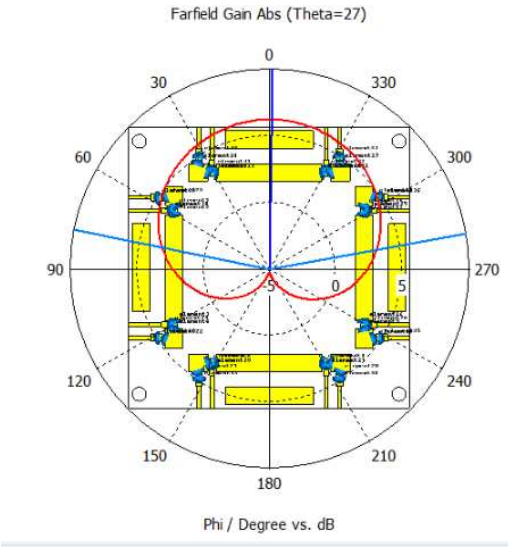

(a)

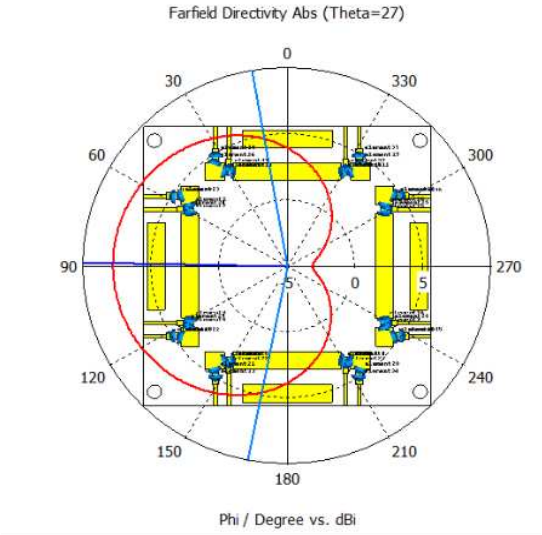

(b)

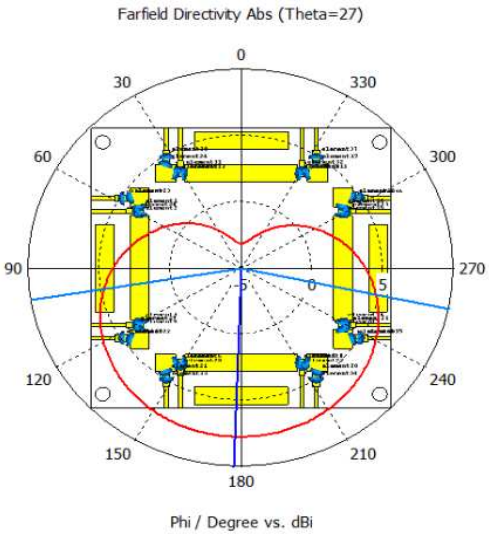

(c)

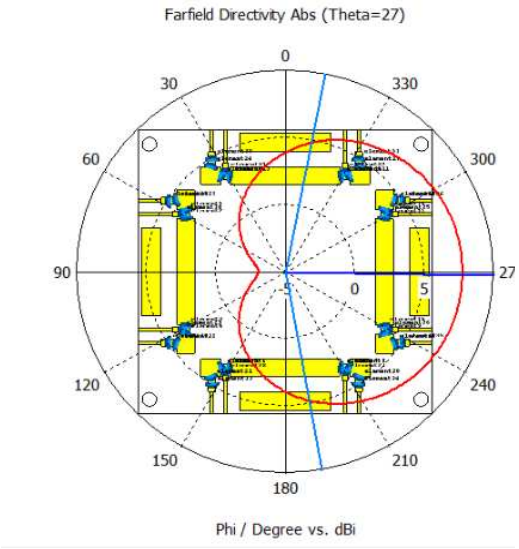

(d)

Figure 3.11 Polar plot of the multi-layered switchable beam antenna radiation pattern showing beam steering in the azimuth plane with a cut angle of θ = 27° (a) φ = 0 (+x), (b) φ = 90 (+y), (c) φ = 180° (-x), (d) φ = 270° (-y)

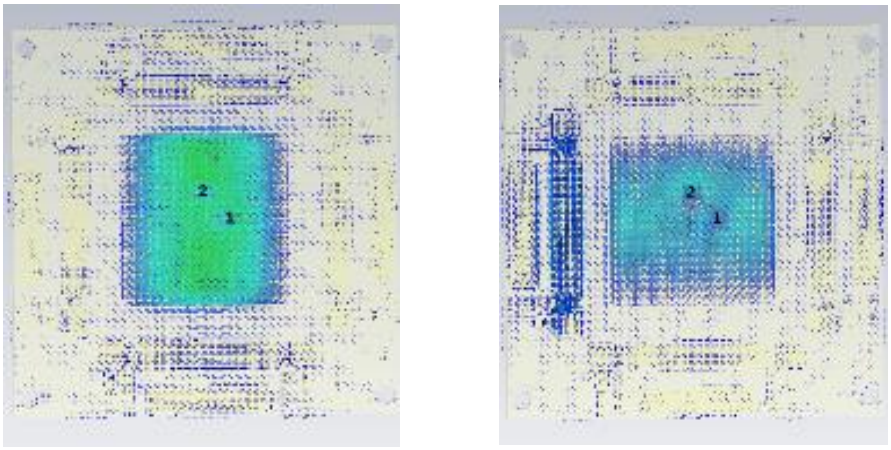

(a) (b)

Figure 3.12 The surface current density of the antenna (a) when all the switches are OFF, (b) when the switches on the left side are ON

Table 3.4 Multi-layered switchable beam antenna results for different beam steering angles. Φ (azimuth), Θ (elevation).

φ	Θ	Directivity (dBi)	Gain (dB)	The angular width of the lobe	Efficiency %
0°	**27°**	7.73	6.18	69.4°	80.63
90°	**27°**	7.75	6.19	69.4°	80.63
180°	**27°**	7.73	6.18	69.4°	80.63
270°	**27°**	7.75	6.19	69.4°	80.63
0°	**0°**	7.71	6.28	76.9°	84.43

3.2.3 Experimental Results

To validate the results, the multi-layer switchable beam antenna layout was fabricated using the PCB rapid prototyping machine ProtoMat S103 shown in Figure 3.13. The fabricated antenna is displayed in Figure 3.14 to Figure 3.18. The Rohde and Schwarz Network analyzer was used to measure the S-parameters of the fabricated antenna. The graphs comparing the simulated and measured S-parameter results for the two-ports system are reported in Figure 3.19 to Figure 3.20, the results were found to be close. There are slight differences in the resonant frequency range (about 30 MHz) and return loss largely as a result of fabrication errors and soldering residue that were not accounted for during simulation. S-parameters below -15 dB depict good input impedance matching therefore very low power loss is achieved. Practical verification of beam steering results requires anechoic chamber measurements. Since we do not have the facility, the measurement results for beam steering are not available now but we plan to get it done in the future in another institution.

Figure 3.13 ProtoMat S103

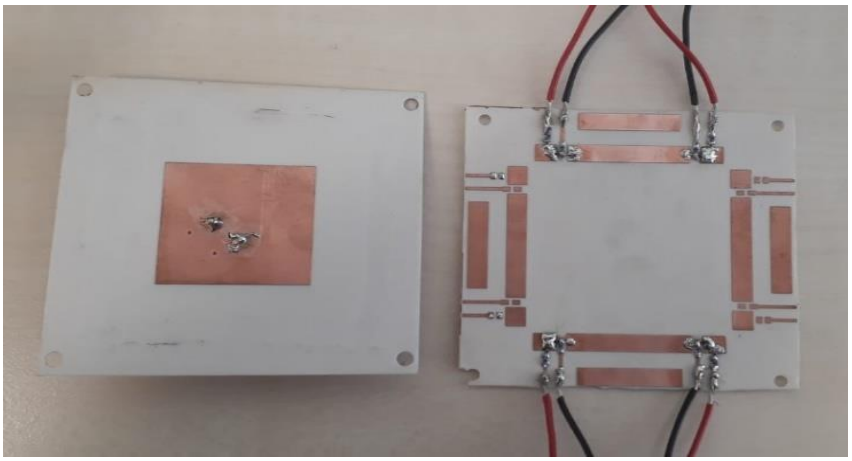

Figure 3.14 Top sides of the active and parasitic layers of the fabricated antenna

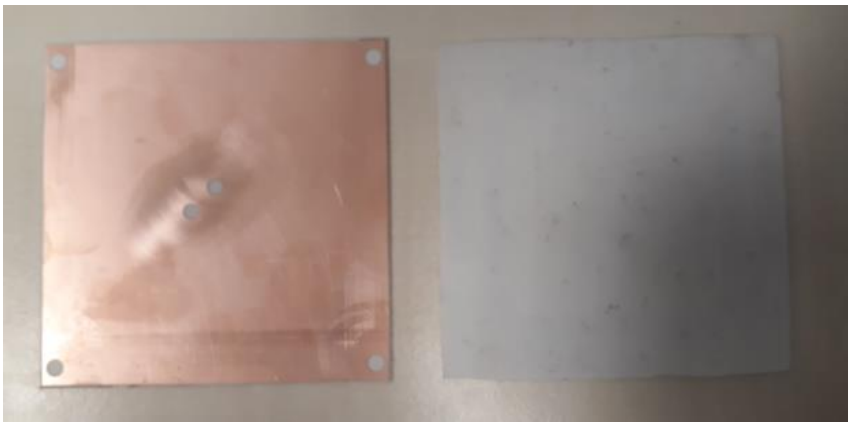

Figure 3.15 Bottom sides of the active and parasitic layers of the fabricated antenna

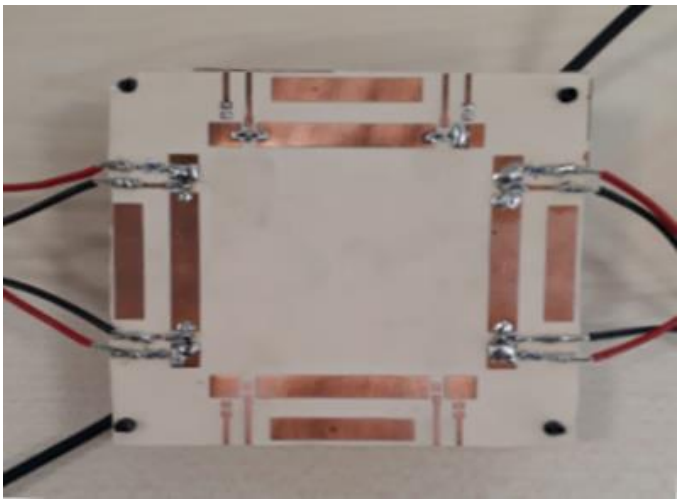

Figure 3.16 Top view of the fabricated antenna

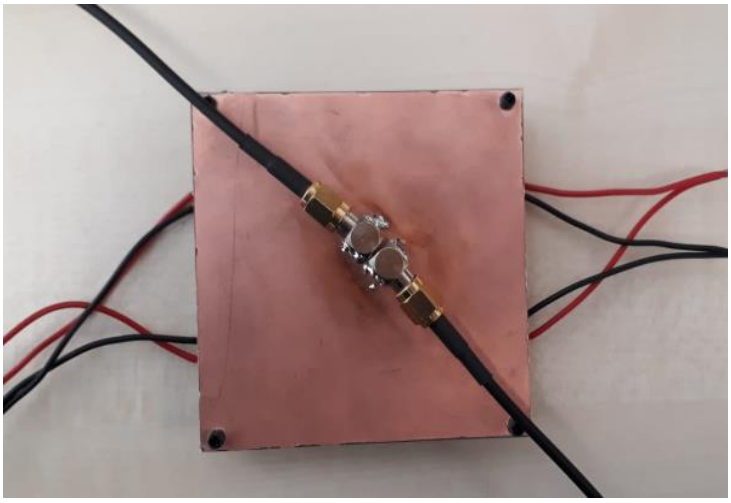

Figure 3.17 Bottom view of the fabricated antenna

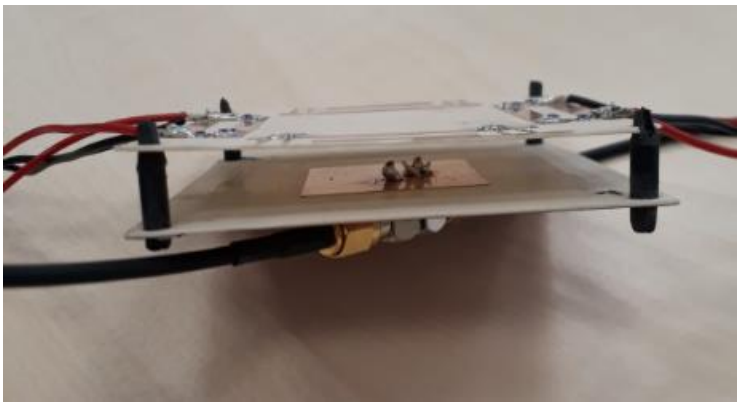

Figure 3.18 Side view of the fabricated antenna

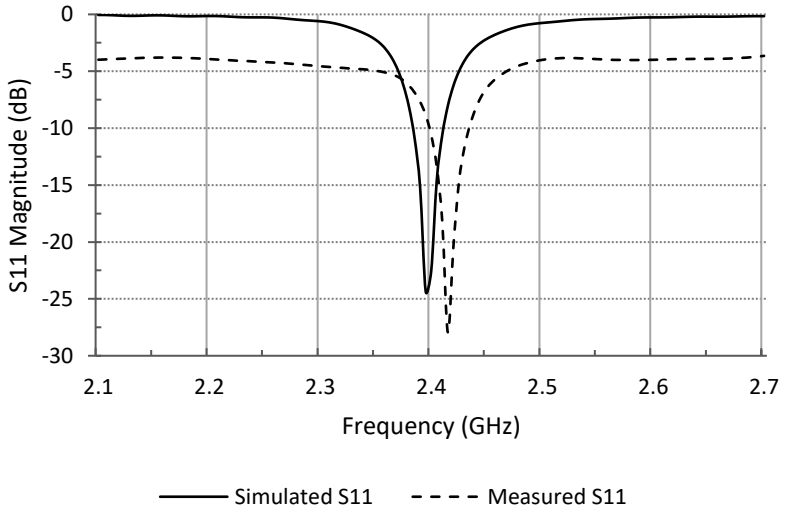

Figure 3.19 Simulated and Measured S11 values (return loss)

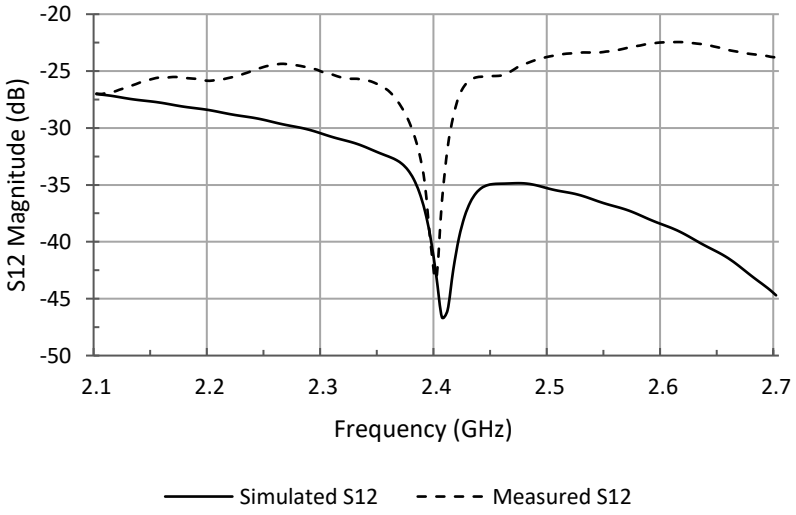

Figure 3.20 Simulated and Measured S12 values (inter-port isolation)

3.2.4 Analysis and Discussion

From detailed simulation and measurement, the effect of the parasitic layer and several parameters on the square patch antenna is observed. The return loss obtained for the antenna for any switch state was below -20 dB, this shows a very

efficient system with low loss. S21 and S12 representing the transmission of signals between the two ports were below -40 dB, this indicates high inter-port isolation which expands the functionality of the antenna by allowing both the transmission and reception of RF signals simultaneously eliminating the need for a complex system such as circulators and antenna cancellers. The parasitic layer consisting of reflectors and directors and controlled by PIN-diodes can steer the radiation beam from one direction to another. Changing the states of the switches only affects the operating frequency by a few megahertz as a result of the radiating beam coupling with the inductors (RF choke) and capacitors (DC block). The operating frequency, the angle of beam steering, and gain are greatly affected by parameters like the height of the air medium and the values of the lumped elements used for biasing. An increase in the resonant frequency is observed when any of the switches are ON and the antenna beam is being steered, this implies that the parasitic layer loads the active antenna inductively when the switches are turned ON.

Compared to the antenna presented in [14] that makes use of two active elements, the proposed antenna uses only one active element and is also able to provide beam steering in four directions with a higher gain of 6.28 dB compared to 5.4 dB that was obtained for the antenna design presented. The antenna in [17] utilizes twenty PIN diode switches and is capable of achieving three steering angles while the proposed antenna operates with only eight switches and steers the beam both in the vertical and horizontal planes in four directions. Table 3.5 compares our proposed design with other antennas presented in the literature. It can be observed that although some of the antennas that are being compared to the proposed antenna have some advantages over the proposed antenna in some aspects such as a higher number of beam steering angles in [3], the antenna in [14] that uses only one switch to achieve the same number of beam steering angles and a higher gain achieved in paper [17], the overall performance and design of the proposed antenna is better when all the factors are taken into consideration.

Table 3.5 Proposed antenna compared with similar antenna designs

Ref	**Freq GHz**	**No. of switches**	**No. of active antenna elements**	**No. of steering beam angles**	**Gain dB**	**Full-duplex capability**
[3]	5.8	8	8	8	4.07	NO
[14]	2.4	1	2	4	5.4	NO
[17]	5.6	20	1	3	8.6	NO
[57]	1.8	4	1	4	4.43	NO
Proposed	2.4	8	1	4	6.28	YES

CHAPTER 4

A 2X2 PATCH ANTENNA ARRAY WITH AN EBG STRUCTURE

The antenna proposed in this Chapter is a 2x2 rectangular microstrip patch antenna array with an Electromagnetic bandgap (EBG) structure. This antenna consists of a 2x2 rectangular patch antenna array with a modified ground plane fed by coaxial probe feedlines. A rectangular patch antenna with an EBG ground plane is first designed and compared to a rectangular patch antenna without the EBG structure at the ground plane, work similar to this has been presented in [12]. The square-shaped hole was used as the unit cell of the EBG structure, the unit cell was then repeated to create a 3x3 array-like structure with uniform spacing. The dimension of the unit cell and the distance between the cells significantly affect the operating frequency of the antenna, therefore they are designed and optimized to work at the required frequency.

The antenna with the EBG structure when simulated had a much lower resonant frequency, this implies an increase in the electrical length of the antenna. To shift the resonant frequency to 2.4 GHz, only the patch length was reduced since shortening the width will lead to a decrease in bandwidth. Better performance was also noticed as there were improvements in gain and bandwidth. The same design idea is then applied to a 2x2 rectangular patch antenna array and compared with a typical version without the EBG structure on the ground plane.

4.1 Rectangular patch with EBG

The rectangular patch antenna with a conventional ground plane is first designed on an FR-4 substrate with a relative permittivity of 4.5 and thickness of 1.5 mm using ((6) (11). Copper metal (0.035 mm thickness) is used for both the patch

and the ground plane. The calculated width and length values for the patch are 29.65 mm and 37.02 mm respectively.

The complexity of EBG structures makes it difficult to characterize them using purely analytical methods. Usually, in EBG analysis, full-wave simulation software based on advanced mathematical methods are used. The EBG structure in this design was initially designed using equations (12 and (13 [12], then the optimization tool is used to obtain the dimensions that produced good return loss at the required frequency. The EBG unit cell designed is an 11x11 mm^2 square-shaped slot etched on the ground plane of the antenna separated by a distance of 7 mm and repeated in a periodic pattern as seen in Figure 4.2(b). The shape, size of the unit EBG cell, and the distance between cells greatly affect the antenna's performance. The feeding port of the antenna was positioned to obtain the best impedance matching without being too close to the slots. The optimized parameters can be seen in Table 4.1.

Inserting the known values into(6) (11), the unknown parameters are calculated below;

$$W = \frac{3x10^8}{2 \times 2.4 \times 10^9 \sqrt{\frac{(4.7 + 1)}{2}}} = 37.02\, mm$$

$$\varepsilon_{reff} = \frac{4.7 + 1}{2} + \frac{4.7 - 1}{2}\left[1 + 12\frac{1.6}{37.02}\right]^{-\frac{1}{2}} = 4.35$$

$$\Delta L = 0.142\frac{\left(\frac{37.02}{1.6} + 0.264\right)(4.35 + 0.3)}{(4.35 - 0.258)\left(\frac{37.02}{1.6} + 0.8\right)} = 0.1578\, mm$$

$$L = \frac{3x10^8}{2 \times 2.4 \times 10^9\sqrt{4.35}} - (2 \times 0.1578) = 29.65\, mm$$

$$\lambda = \frac{c}{f} = \frac{3 \times 10^8}{2.4 \times 10^9} = 125\, mm$$

$$\lambda_g = \frac{3 \times 10^8}{2.4 \times 10^9 \sqrt{4.35}} = 60\ mm$$

$$w = 0.10\ \lambda \tag{12}$$

$$g = 0.02\ \lambda \tag{13}$$

$$w = 0.10 \times 125 = 12.5\ mm$$

$$g = 0.02 \times 125 = 2.5\ mm$$

Table 4.1 Parameters of the rectangular patch without and with EBG

Parameter	Patch without EBG structure	Patch with EBG structure
W1 (Width and length of the ground)	60 mm	60 mm
Wp (Width of the patch)	37 mm	37 mm
Lp (Length of the patch)	28.5 mm	23 mm
We1 (Width of the EBG hole)	NA	11 mm
g1 (Distance between the EBG holes)	NA	7 mm

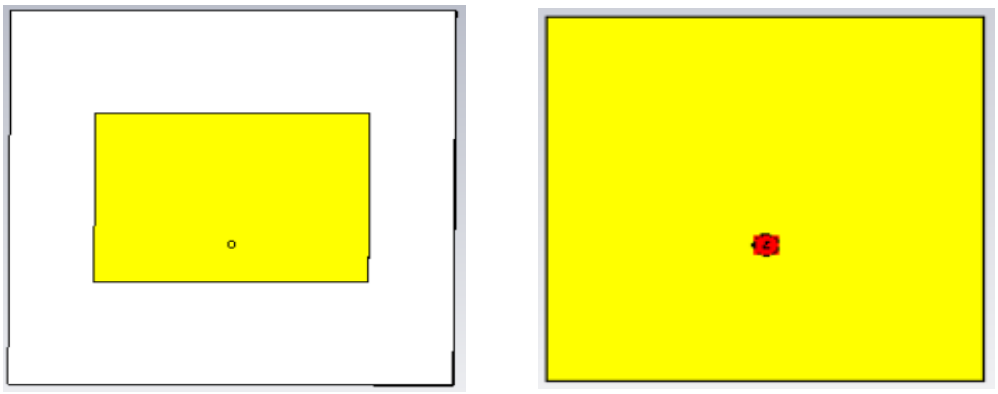

(a) (b)

Figure 4.1 Rectangular patch antenna without EBG; a) Top view and b) Bottom view

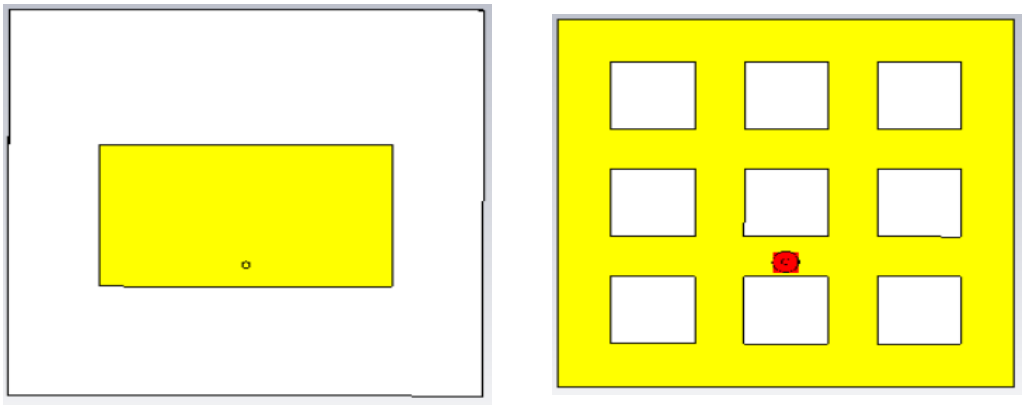

(a) (b)

Figure 4.2 Rectangular patch antenna with EBG; a) Top view and b) Bottom view

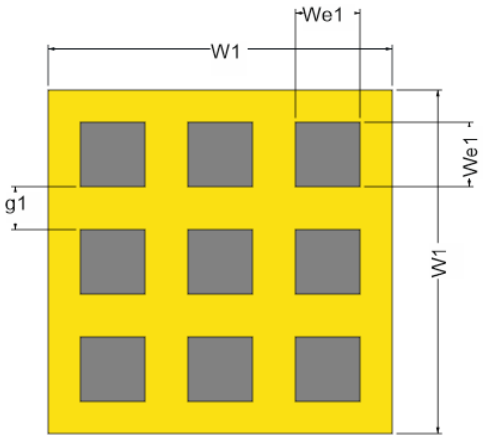

Figure 4.3 The EBG structure

4.1.1 Numerical analysis

The rectangular patch antenna is simulated and optimized using CST microwave studio. The calculated values for the antenna dimensions are used for the initial antenna design before simulation. The antenna parameters and the position of the feeding ports are then optimized so that the antenna can operate at the required frequency. To obtain the optimized dimensions of w and g, the optimization tool in CST was used to simulate the results for various w and g dimensions, and the optimal w and g dimensions were obtained at a frequency of 2.4 GHz.

The 3-D far-field patterns of both antennas showing the gain values are illustrated in Figure 4.4, the antenna gain increased from 3.33 dB to 4.03 dB when the EBG structure is included in the ground plane. Incorporating the EBG holes into the ground layer as discussed above reduced the surface wave propagation of the antenna resulting in a higher gain value (surface wave propagation of an antenna leads to lower efficiency). Figure 4.5 and Figure 4.6 show the simulated S11 parameters of the microstrip patch antenna without and with EBG respectively. There is a decrease in the resonant frequency from 2.4 GHz to 2.03 GHz that is a result of the electrical length of the antenna increasing. To obtain the same frequency as the patch without EBG, the overall area of the patch has to be reduced leading to the miniaturization of the antenna. The width of the antenna was left unchanged to avoid reducing the bandwidth of the antenna while the length was reduced from 28.5 mm to 23 mm which is a 19.3 % reduction in overall antenna area. The obvious size difference can be seen in Figure 4.1 and Figure 4.2. The effect of reducing the length of the antenna is shown in Figure 4.7, the operating frequency shifted from 2.03 GHz to 2.4 GHz. A wider bandwidth is another significant improvement introduced by the EBG structure. The simulated 10-dB bandwidth increased from 73.5 MHz to 109.1 MHz when the structure was added. The directivity value of the antenna with EBG is lower than that of the antenna with EBG, this is an expected result because of the increase in the bandwidth of the antenna with EBG. The increase in antenna gain can be justified by observing the beamwidth of both antennas. The angular

beamwidth (which is inversely proportional to the antenna gain) of the antenna with EBG is less than that of the antenna without EBG, this means that the same amount of power is focused on a reduced area thereby increasing the antenna gain. There was also a trade off in the antenna efficiency to achieve these improvements mainly as a result of the increase in the back lobe.

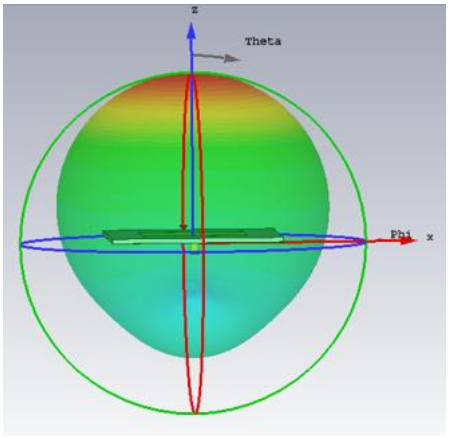

(a)

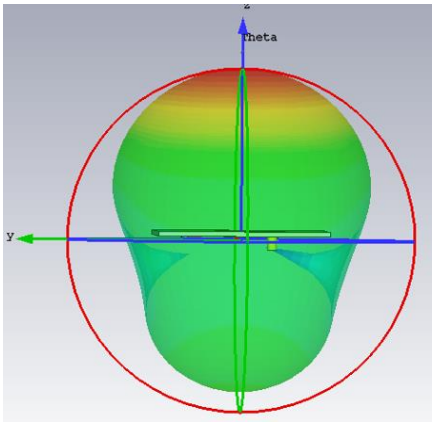

(b)

Figure 4.4 Far-field plot showing the gain values of rectangular patch antenna (a) without EBG (b) with EBG

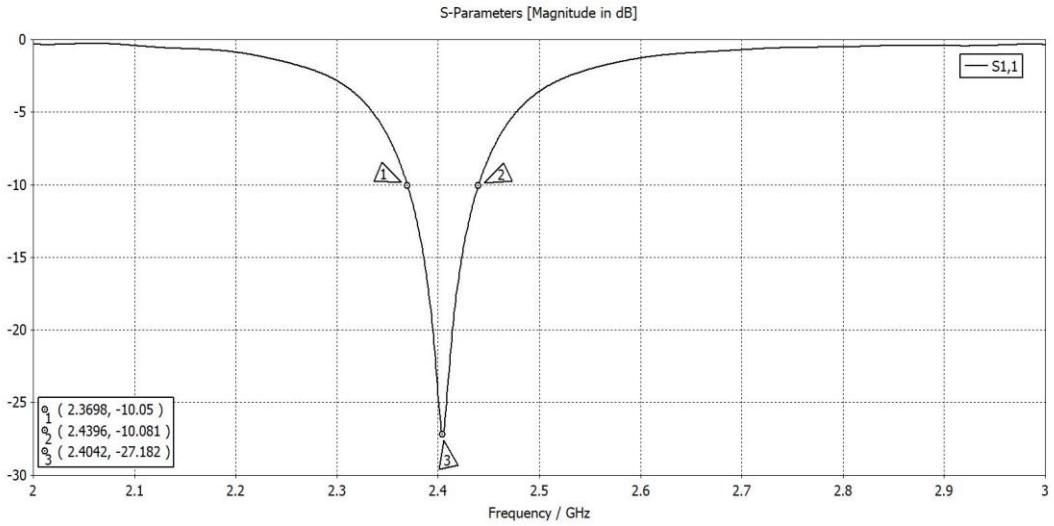

Figure 4.5 S-Parameter result for the rectangular patch antenna without EBG

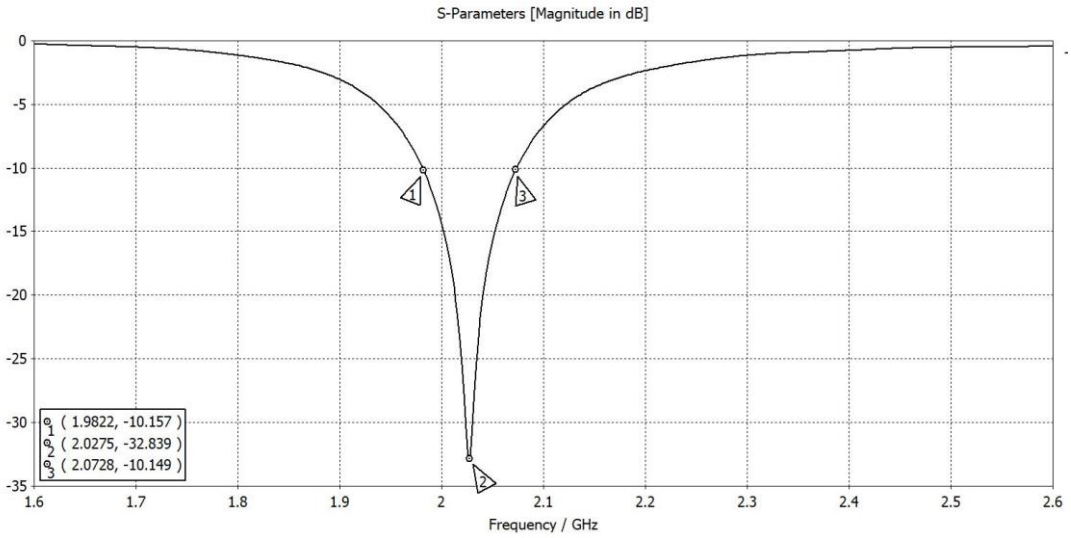

Figure 4.6 S-Parameter result for the rectangular patch antenna with EBG showing a shift in the resonant frequency from 2.4 GHz to 2.0283 GHz

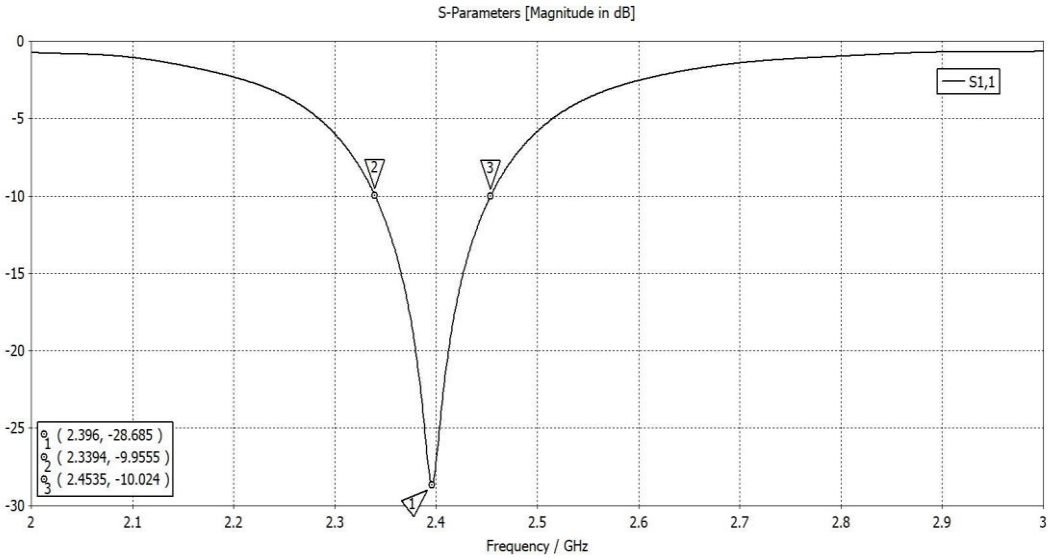

Figure 4.7 S-Parameter result for the rectangular patch antenna with EBG after reducing the size of the antenna to achieve 2.4 GHz

Table 4.2 Comparison between the single patch antenna without and with EBG

	Antenna without EBG	Antenna with EBG
Gain (dB)	3.33	4.03
Directivity (dBi)	6.52	5.77
Bandwidth (MHz)	73.5	109.1
Angular beamwidth (deg.)	92.9	80.1
Length (mm)	28.5	23
Width (mm)	37	37

4.2 Antenna Array with EBG

A single element's radiation pattern is relatively broad, and each element provides low values of directivity and gain. To meet the demands of long-distance communication, many applications, particularly point-to-point communication

systems, require antennas with very directive characteristics (high gain). This can be achieved by increasing the antenna's electrical size. Arrays are incredibly flexible and adaptable and are used to produce necessary radiation patterns which cannot be realized with a single element, among other things. They can also be used to scan an antenna system's beam, increase directivity, and perform a variety of other tasks that would be difficult to execute with a single element. Planar arrays are more versatile and can generate symmetrical patterns with lower side lobes.

Coupling between microstrip antenna arrays has always been a problem, resulting in surface wave formation, reduced antenna performance, and pattern shape disruption. Meta-materials have been utilized to reduce coupling between arrays in the substrate of rectangular patch antenna arrays to solve this problem [58], hence the use of EBG structures for the proposed antenna.

4.2.1 Antenna Design

To demonstrate the performance of the 2x2 antenna array with EBG structure on the ground, a typical antenna array without EBG working at the same frequency of 2.4 GHz is designed and simulated. The 2x2 antenna array with a conventional ground plane consists of four rectangular patch antenna elements with each patch having a dimension of 37 x 28.3 mm^2 and the ground plane 180 x 160 mm^2. The antenna array shown in Figure 4.8 is designed on an FR-4 substrate which has a dielectric constant $\varepsilon r = 4.7$. The separation between the patch elements in the H-plane and the E-plane is always between $\lambda/2$ to λ. CST optimization tool was used to obtain the performance of the antenna between $\lambda/2$ to λ. The distance along the E-arm and H-arm is kept constant at the optimal value of return loss. Each element of the antenna array is fed by a coaxial probe.

The 2x2 patch antenna array with EBG is shown in Figure 4.9. The unit element of the antenna array with EBG was designed using the same dimensions as the single patch antenna with EBG. The width and length measurements are 37.02

mm and 23.5 mm respectively. The proposed antenna is also fabricated on an FR-4 substrate with a thickness of 1.5 mm and a relative permittivity of 4.7. The length of the patch was adjusted to obtain response at the required frequency. The feeding ports of the antenna have to be strategically positioned to avoid the holes of the EBG structure and obtain good return loss at the same time. The calculated parameters for the antenna arrays with and without EBG are shown in the table below.

Table 4.3 Dimensions of the antenna array without and with EBG

Parameter	Antenna array without EBG	Antenna with EBG
Length of the patch (mm)	28.3	23.5
Width of the patch (mm)	37	37.2
Inter-element spacing (center-to-center) (mm)	0.833λ	0.833λ
Length of the ground (mm)	150	130
Width of the ground (mm)	180	160

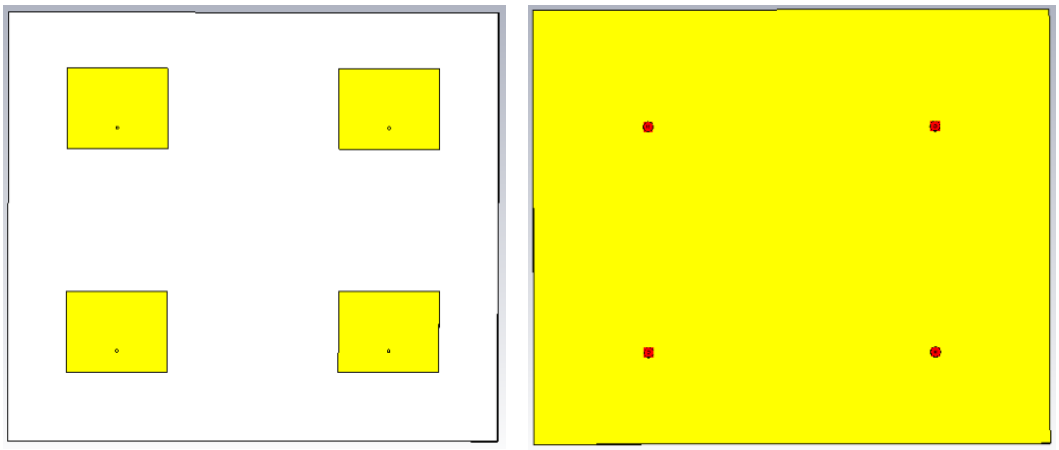

(a) (b)

Figure 4.8 The top and bottom view of the 2x2 rectangular patch array without EBG; a) Top view, b) Bottom view

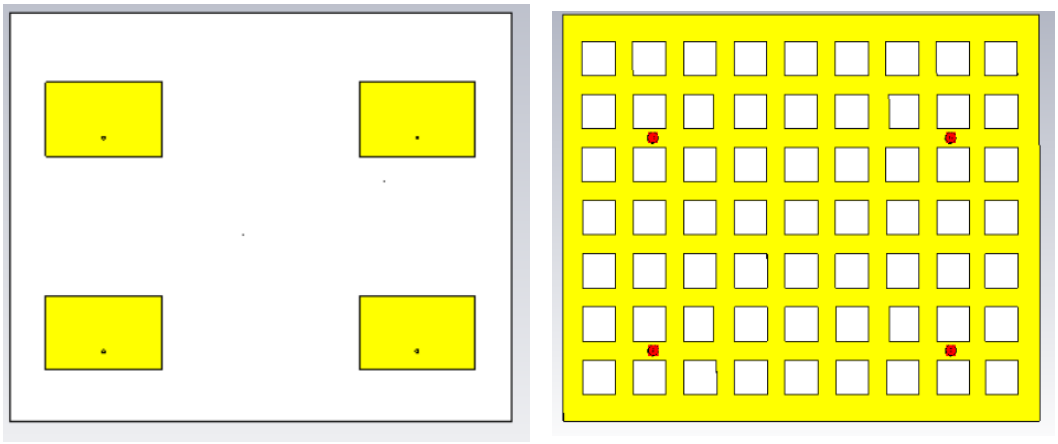

(a) (b)

Figure 4.9 The top and bottom view of the 2x2 rectangular patch array with EBG; a) Top view, b) Bottom view

4.2.2 Numerical analysis

After designing both antenna arrays using theoretical analysis, they are simulated by making use of the time domain solver in CST from 2-3 GHz. This simulation aims to demonstrate the beam steering capabilities of the antenna array and also observe the improvement of antenna array properties after including the EBG structure. The antenna array without EBG is first simulated and optimized to resonate at 2.4 GHz. The S-parameter result is obtained and shown in Figure 4.10. It can be seen that the average return loss for the four ports is -24.793 dB with a 60 MHz bandwidth.

The S-parameter result of the 2x2 antenna array with EBG is shown in Figure 4.11. From the graphs shown, the improvements in the return losses of the four ports are very noticeable. The average return loss value for the four ports increased from -28.52 dB to -40 dB after the EBG structure was added to the design. There was an increase in the bandwidth from 60 MHz to 100 MHz. The overall area of the patch antenna array was also reduced by 32.3% from 180 x 160 mm^2 to 150 x 130 mm^2.

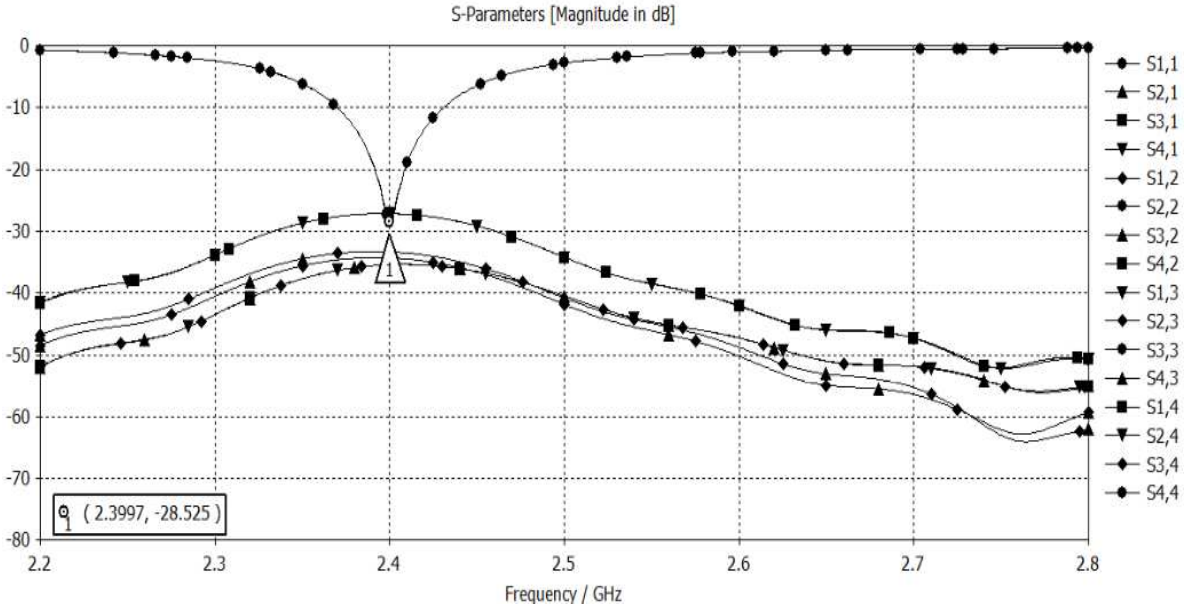

Figure 4.10 S-parameter results of the 2x2 antenna array without EBG

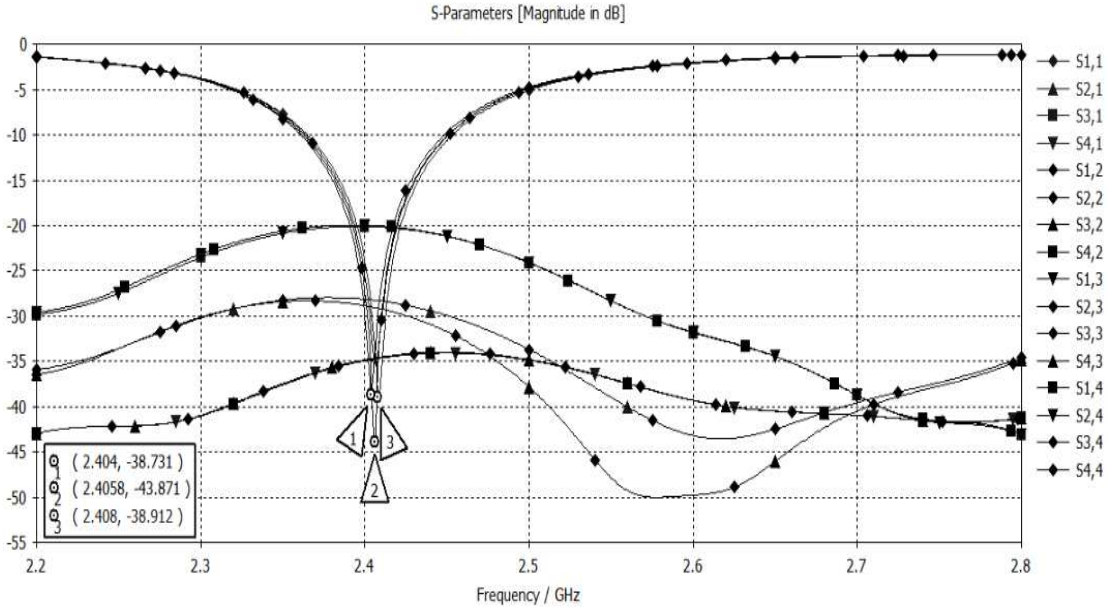

Figure 4.11 S-parameter results of the 2x2 antenna array with EBG

4.2.2.1 Beam steering

There are several scanning techniques that have been used to achieve beam steering of antenna arrays in literature. These include phase scanning, time-delay scanning, frequency scanning and IF scanning [59]. The antenna array with EBG proposed in this research employs the phase scanning technique for beam steering. The direction of the antenna array beam is typically perpendicular to the phase front. To alter the direction of the beam, the phase front is adjusted by individually controlling the phase shift of each antenna element. The phase shifters are controlled electronically to allow for rapid scanning and the values can be adjusted from 0 to 2π. As shown in Figure 4.12 below, the phase shift ψ between adjacent elements for a scan angle of θ_O can be represented as

$$\psi = \frac{2\pi}{\lambda} s \sin\theta_O \qquad \text{Eq 14}$$

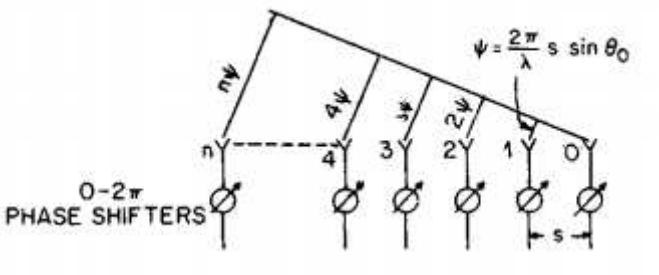

Figure 4.12 Phase scanning in antenna arrays [59]

The goal of adaptive beamforming is to change the beam by trying to adjust the gain and phase on each element of the antenna in order to form a highly desired pattern. [44]. To provide the necessary phase shifts and amplitude for each port of the antenna in CST, the "combine results" option under the "post processing" menu is selected. This feature offers the possibility of calculating fields for the excitation specified inside CST. Figure 4.13 to Figure 4.15 shows the CST settings used to control the phase shift and amplitude of the excitation signals and the resulting far-field plot of the antenna.

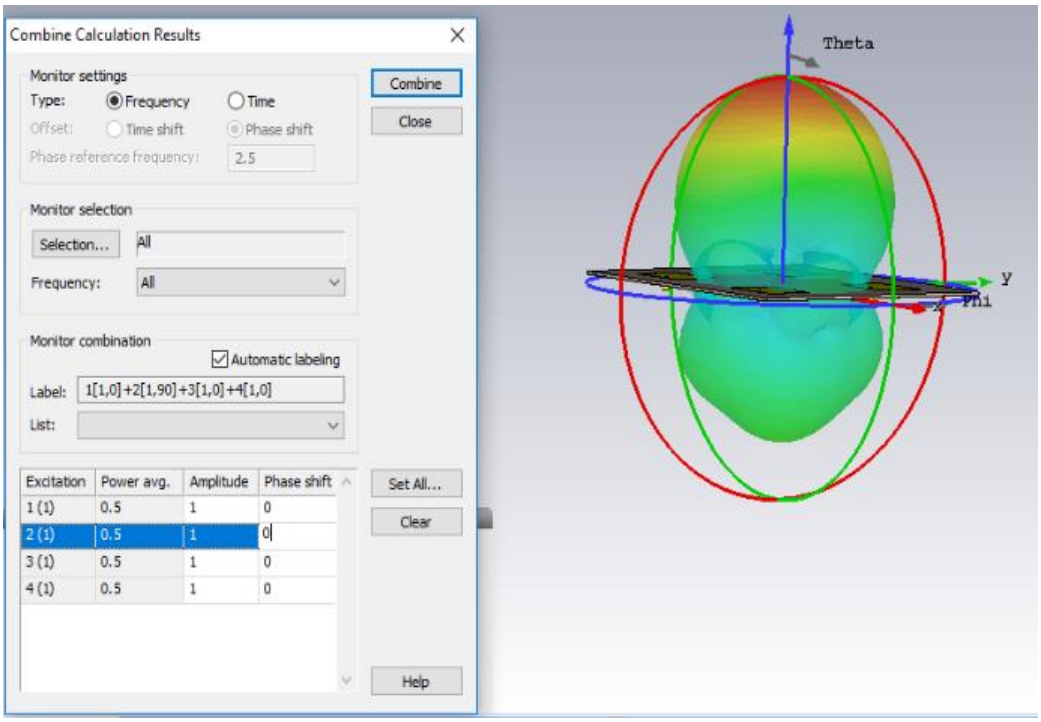

Figure 4.13 Resulting far-field result for all ports excitation with no phase shifts

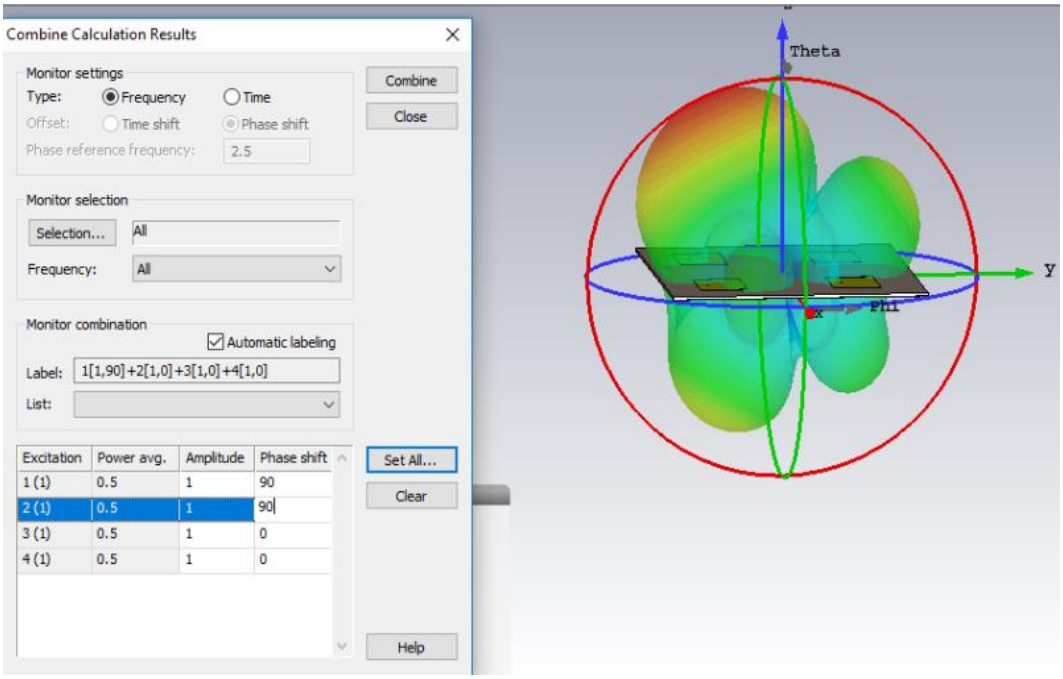

Figure 4.14 Resulting far-field result for all ports excitation with 90° phase shifts in ports 1 and 2

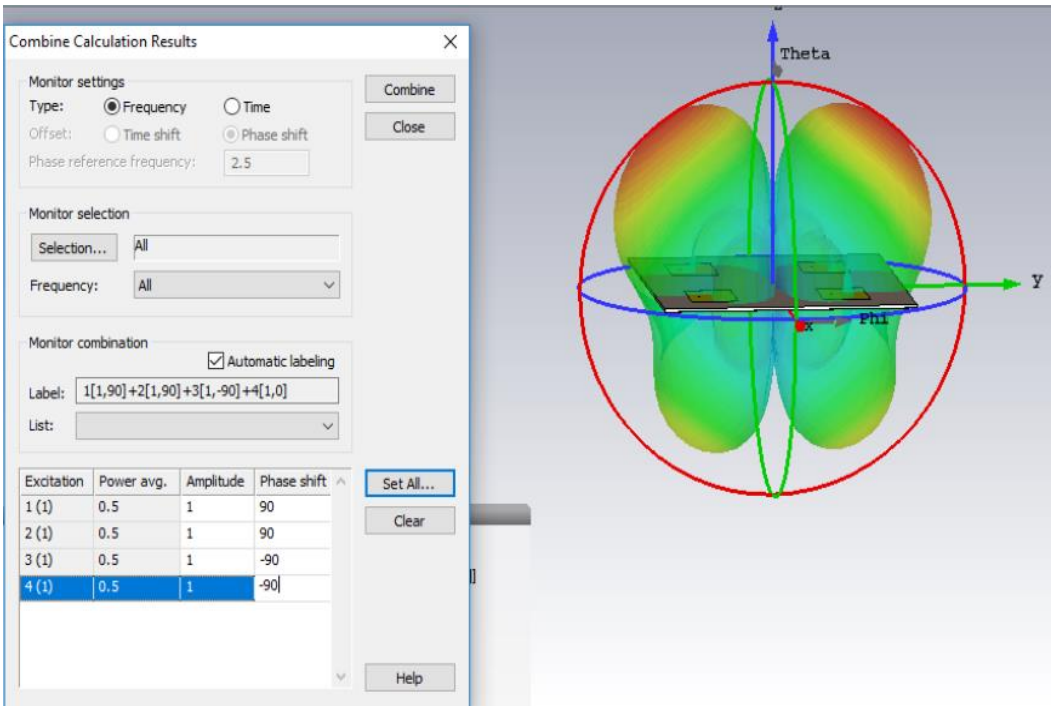

Figure 4.15 Resulting far-field result for all ports excitation with 90° phase shifts in ports 1 and 2 and -90° phase shifts in ports 3 and 4

The polar plots illustrating the beam steering process are shown in Figure 4.16. Depending on the phase shift and amplitude of the excitation signals of the four ports, beam steering angles of 0 to 36 degrees can be achieved. Larger steering angles produce very large side lobes which reduce the efficiency of the antenna. The maximum gain which is 8.8 dB is obtained from the 2x2 antenna array with EBG when the beam is steered at an angle of 24°. The average directivity value of the antenna array with EBG is lower than the antenna array with EBG, this is an expected result due to the increase in bandwidth of the antenna with EBG. Table 4.4 and Table 4.5 provide the gain and directivity values for different beam steering angle for the antenna array with and without EBG respectively.

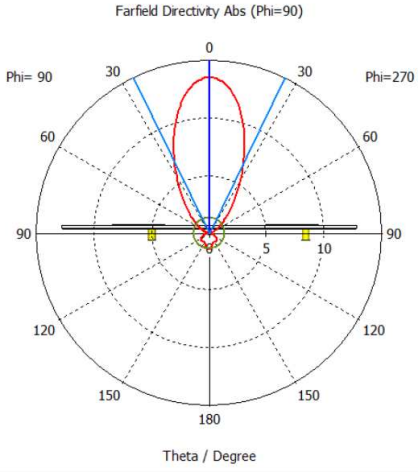

(a) 0° beam steering

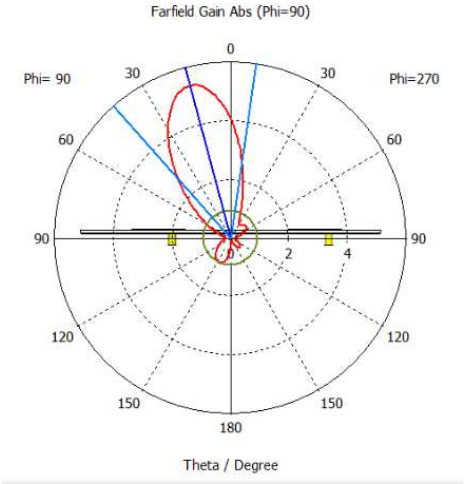

(b) 15° beam steering

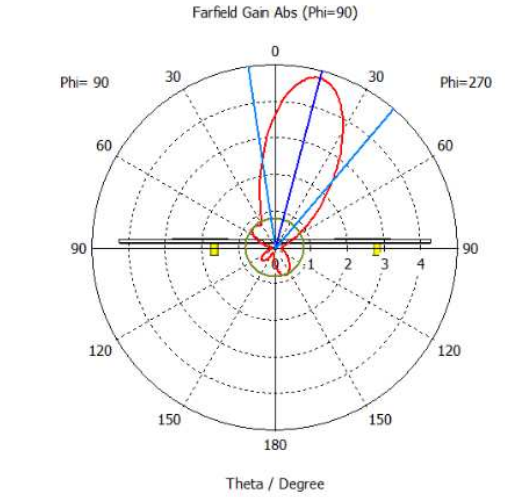

(c) -15° beam steering

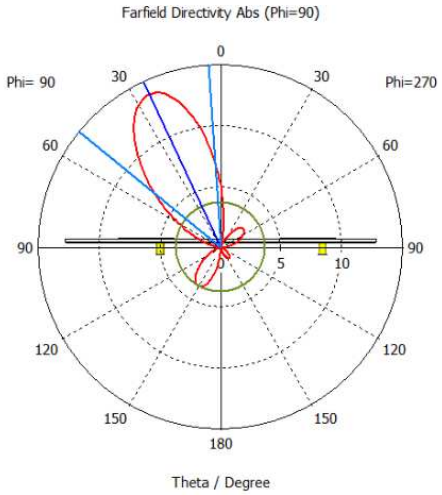

(d) 25° beam steering

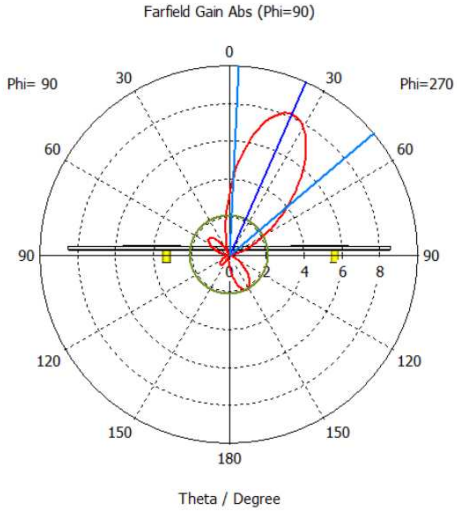

(e) -24° beam steering

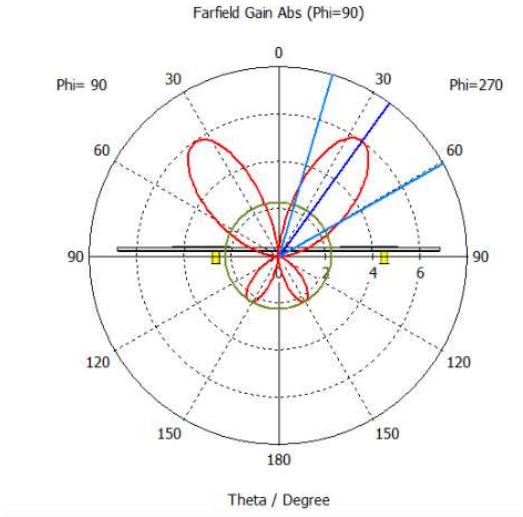

(f) ±36° beam steering

Figure 4.16 Polar plots of the 2x2 antenna array with EBG showing beam steering from -36° to 36°

Table 4.4 Simulation results for the 2x2 antenna array with EBG

Port [phase shift]	Beam-steering angle (θ)	Gain (dB)	Directivity (dBi)
1[0], 2[0], 3[0], 4[0]	0	7.8	11.5
1[90], 2[0], 3[0], 4[0]	-15	7.42	10.6
1[0], 2[0], 3[0], 4[90]	15	7.37	10.6
1[90], 2[90], 3[0], 4[0]	-24	8.8	11.5
1[0], 2[0], 3[90], 4[90]	25	8.76	11.5
1[90], 2[90], 3[-90], 4[-90]	±36	7.41	9.33

Table 4.5 Simulation results for the 2x2 antenna array without EBG

Port [phase shift]	Beam-steering angle (θ)	Gain (dB)	Directivity (dBi)
1[0], 2[0], 3[0], 4[0]	0	7.96	13.2
1[90], 2[0], 3[90], 4[0]	-15	7.41	12.4
1[0], 2[90], 3[0], 4[90]	15	7.41	12.4
1[90], 2[90], 3[0], 4[0]	-21	8.09	12.5
1[0], 2[0], 3[90], 4[90]	18	7.95	12.3
1[90], 2[90], 3[-90], 4[-90]	±37	7.09	10.7

4.2.3 Experimental Results

The 2x2 antenna array with EBG is printed using the PCB rapid prototyping machine, the S-parameter results are measured with the Rohde and Schwarz Network analyzer and then compared with the simulated S-parameter results. The top and bottom views of the fabricated antenna are shown in Figure 4.17 and Figure 4.18. The graphs comparing the simulated and measured S-parameter results for the antenna array with EBG are reported in Figure 4.19 to Figure 4.22, the results are found to be in close agreement. The return losses are below -30 dB which depict very good input impedance matching therefore very low power loss is achieved. Practical verification of beam steering results requires anechoic chamber measurements. Since we do not have the facility, the measurement results for beam steering are not available now but we plan to get it done in the future in another institution.

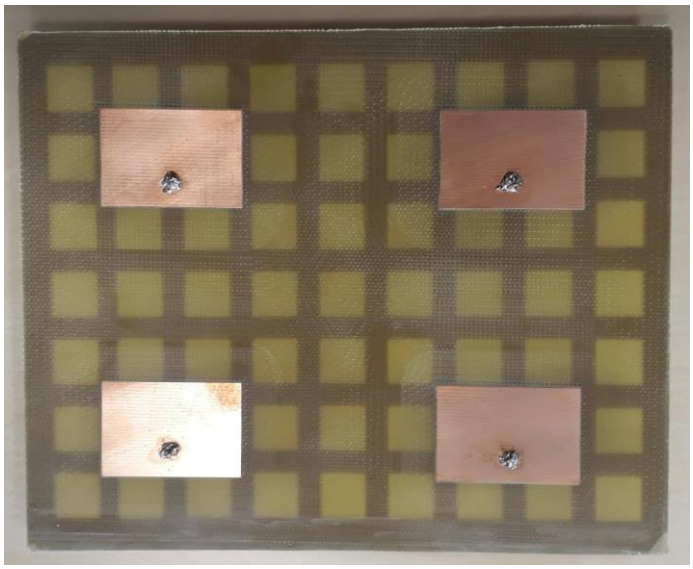

Figure 4.17 Top view of the 2x2 antenna array with EBG

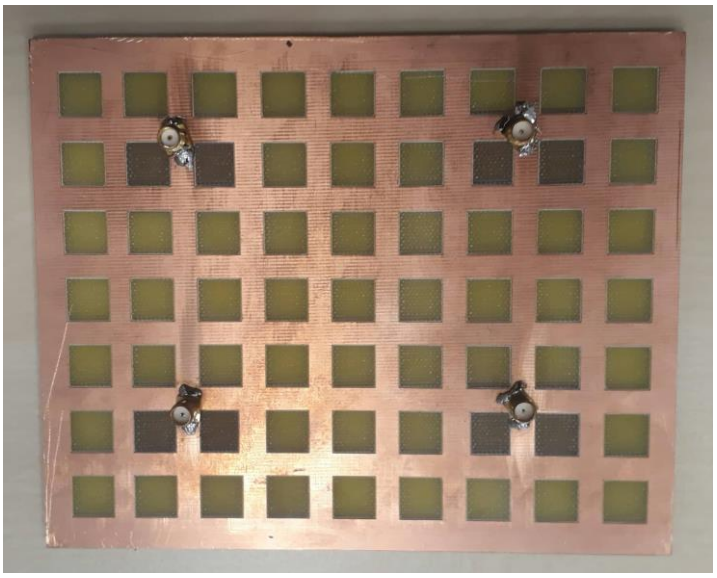

Figure 4.18 Bottom view of the 2x2 antenna array with EBG

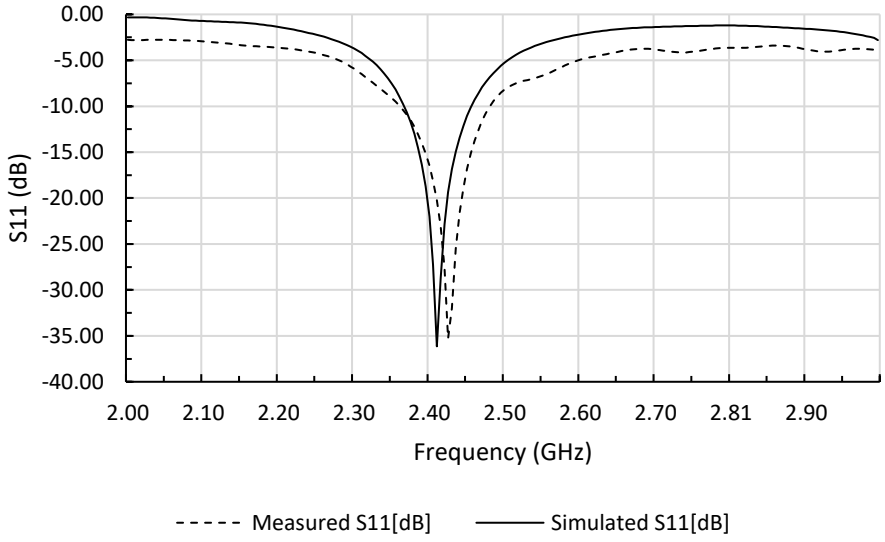

Figure 4.19 Measured and Simulated S11 results of the 2x2 antenna array with EBG

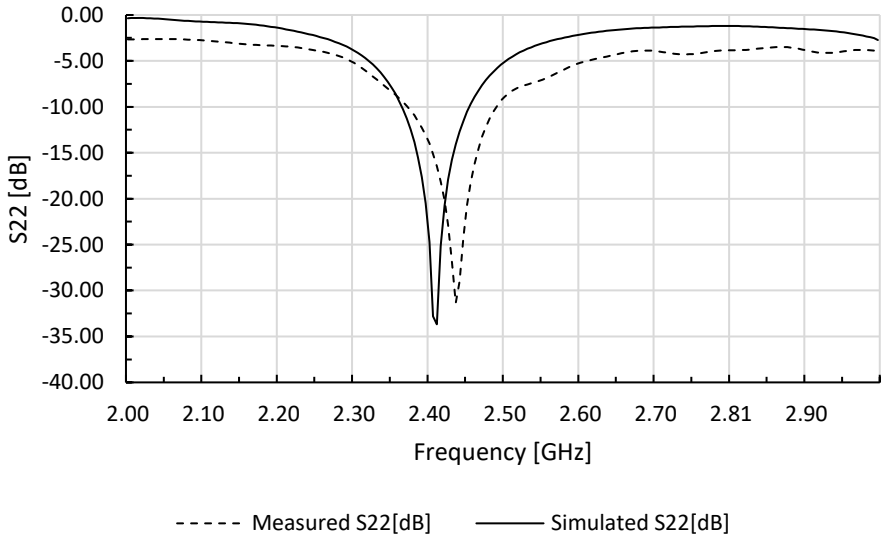

Figure 4.20 Measured and Simulated S22 results of the 2x2 antenna array with EBG

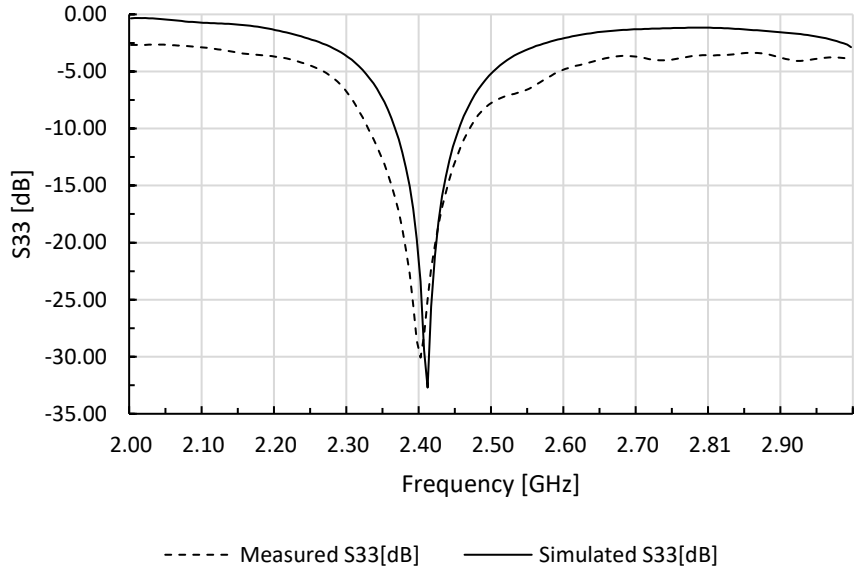

Figure 4.21 Measured and Simulated S33 results of the 2x2 antenna array with EBG

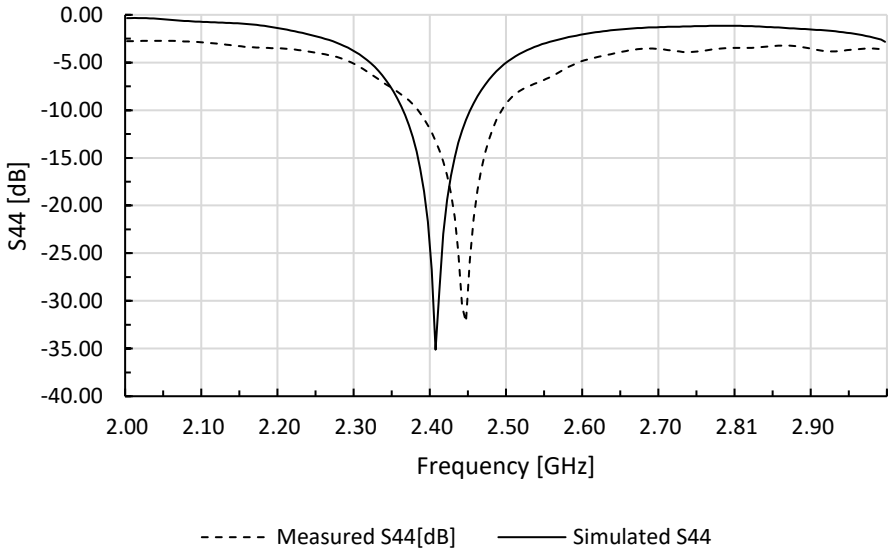

Figure 4.22 Measured and Simulated S44 results of the 2x2 antenna array with EBG

4.2.4 Discussion

The comparison between the results and dimensions of both antennas is summarized in Table 4.6. The effects of the EBG ground in the antenna array are observed. The return loss of the antenna with EBG ground in dB is approximately two times more than the return loss of the antenna with the conventional ground plane. This shows that there is less loss experienced by the antenna with the EBG ground which is largely due to less coupling between antenna elements and reduced surface wave formation. From the S-parameters result, the 10-dB bandwidth of the antenna array with EBG ground is measured and is observed to be 40 MHz larger than the bandwidth of the conventional antenna array. A maximum gain of 9.1 dB is obtained from the antenna with EBG at 25° beam steering. Both the improvements in the gain and bandwidth of the antenna are also due to surface wave suppression offered by the EBG structure. Another major benefit of the EBG structure is the miniaturization of the antenna array. Introducing the EBG structure increased the electrical length of the antenna which in turn shifted the frequency much lower than the operating frequency. To move the frequency back to 2.4 GHz, the physical length is reduced by 32.3%. Although better gain and bandwidth results are obtained, these improvements are achieved at the cost. There was a trade-off between achieving a higher bandwidth and lower directivity. For IoT applications, the overall antenna performance is sufficient.

Table 4.6 compares the proposed antenna to other 2x2 antenna array with EBG structure that has been presented in the literature. It is observed that compared to other antenna designs, the proposed antenna is the only antenna that has achieved both beam steering and miniaturization. It also has the highest percentage bandwidth increase of 66%.

Table 4.6 Simulation results comparing the 2x2 antenna array without and with EBG

	Array without EBG	Array with EBG
Return loss (S11)	-24.685	-50.08
Bandwidth (MHz)	60	100
Antenna array size	180x160	150x130
Maximum gain	8.48	9.1
Highest directivity	13.2	11.4

Table 4.7 Proposed antenna compared with similar antenna designs

Ref	**Peak gain**	**Peak directivity**	**% BW increase**	**% Reduction in return loss**	**% Size reduction**	**Beam steering capability**
[11]	6.5	8.5	39.63	59.7	22.38	No
[18]	13.5	14.2	No increase in BW	43.5	No size reduction	No
[19]	7.87	9.83	30	50	No size reduction	Yes
Proposed antenna	9.1	11.4	66	45	32.3	Yes

CHAPTER 5

CONCLUSION AND FUTURE WORK

5.1 CONCLUSION

In this thesis, two switchable and steerable beam antennas operating within the ISM frequency band are proposed. The microstrip patch antenna type is used for both antennas to achieve simple, compact, light-weight and inexpensive designs which are part of the requirements in this research.

Beam steering is achieved in the multi-layered switchable beam antenna by electronically controlling the PIN diode switches placed on the Yagi-Uda parasitic layer. The active patch was initially fed by one coaxial feedline but was only able to achieve beam steering in two directions, introducing the second feedline made beam steering in four directions possible. Due to the orthogonal polarization of the antenna, high inter-port isolation was realized making it very useful in full-duplex communication applications. The addition of extra directors to the four sides of the parasitic layer increased the directivity and gain of the antenna and improved the steering angle significantly. The proposed antenna also has a simpler design and uses a smaller number of switches compared to many other smart switchable antennas that have been reported. The simulation and measured results agree well and prove that the proposed antenna is capable of achieving high inter-port isolation.

The 2x2 patch antenna array with the EBG consists of four rectangular patch antennas on top of an FR-4 substrate fed by four coaxial feeding ports and a ground plane with an EBG structure. Beam steering from -36° to 36° for the antenna was achieved by changing the amplitude and phase of the four RF supplies. To demonstrate the improvements brought about by the inclusion of the EBG structure, a 2x2 patch antenna with a conventional ground plane operating at the same

frequency was designed and simulated. The results of both antennas showed that there was an increase in the return loss, gain, and bandwidth of the antenna array with the EBG structure. As a result of the increase in the electrical length of the antenna due to the inclusion of the EBG structure, the size of the antenna array was also reduced by 32.3%. After measuring the fabricated antenna, the simulated results show good agreement with the measured results.

The outcome of the work done on the Multi-layered switchable beam antenna was submitted to the Transaction of Antennas and Propagation Journal for publication while the paper for the 2x2 patch antenna array with EBG is under preparation and will also be submitted to the same journal.

5.2 Future Work

Regarding the multi-layered switchable beam antenna, the focus of this research was mainly on the transmitted signals. For future work, a transmit and receive system consisting of the single antenna could be setup to demonstrate the isolation of the two ports. In addition to this, there could be more research on reducing the complexity of the antenna further by reducing the number of PIN-diodes used.

The proposed 2x2 antenna array with EBG utilizes individual phase shifters for each port. To improve this design and make it more compact, phase shifters can be designed on the patch layer using PIN diodes and controlling them electronically. Substituting the FR-4 substrate for a substrate with a lower dielectric constant such as Rogers will reduce losses thereby enhancing the performance of the antenna by improving the bandwidth and gain.

REFERENCES

[1] S. V. S. Nair and M. J. Ammann, "Reconfigurable antenna with elevation and azimuth beam switching," *IEEE Antennas Wirel. Propag. Lett.*, vol. 9, pp. 367–370, 2010, doi: 10.1109/LAWP.2010.2049332.

[2] C. A. Balanis, *Antenna Theroy: Analysis and Design*. 2012.

[3] L. W. Leong, L. Y. Seng, W. F. Hoon, and M. F. A. Malek, "Switchable beam antenna," *RFM 2013 - 2013 IEEE Int. RF Microw. Conf. Proc.*, no. December, pp. 86–89, 2013, doi: 10.1109/RFM.2013.6757224.

[4] S. Zhang, X. Chen, I. Syrytsin, and G. F. Pedersen, "A Planar Switchable 3-D-Coverage Phased Array Antenna and Its User Effects for 28-GHz Mobile Terminal Applications," *IEEE Trans. Antennas Propag.*, vol. 65, no. 12, pp. 6413–6421, 2017, doi: 10.1109/TAP.2017.2681463.

[5] M. Jusoh, M. F. Jamlos, N. M. Nawawi, A. Alomainy, M. R. Kamarudin, and M. R. Hamid, "Switchable parasitic antenna using PIN Diode- and MEMS-switches," *RFM 2013 - 2013 IEEE Int. RF Microw. Conf. Proc.*, pp. 353–355, 2013, doi: 10.1109/RFM.2013.6757283.

[6] N. Haridas *et al.*, "Reconfigurable MEMS antennas," *Proc. 2008 NASA/ESA Conf. Adapt. Hardw. Syst. AHS 2008*, no. July, pp. 147–154, 2008, doi: 10.1109/AHS.2008.28.

[7] Y. Tazaki, E. Nishiyama, and M. Aikawa, "Beam Steering Microstrip Antenna with Varactor Diode," pp. 712–715.

[8] B. Schaer, K. Rambabu, and J. Bornemann, "Beam Steering Arrays," vol. 53, no. 6, pp. 1998–2003, 2005.

[9] T. Beijing, "A Design of Phased Array Antenna Based on the Vivaldi Antenna," pp. 334–337, 2010.

[10] J. W. Baik, S. Pyo, T. H. Lee, and Y. S. Kim, “Switchable printed Yagi-Uda antenna with pattern reconfiguration,” *ETRI J.*, vol. 31, no. 3, pp. 318–320, 2009, doi: 10.4218/etrij.09.0209.0006.

[11] F. Ghorbani, A. Abdi, A. Sahraei, M. Fallahzadeh, H. Aliakbarian, and S. Radiom, “Beam switchable radiosonde receiver antennas,” *AEU - Int. J. Electron. Commun.*, vol. 127, no. August, p. 153442, 2020, doi: 10.1016/j.aeue.2020.153442.

[12] A. Agnihotri, A. Prabhu, and D. Mishra, “Improvement in Radiation Pattern Of Yagi-Uda Antenna,” *Res. Inven. Int. J. Eng. Sci.*, vol. 2, no. 12, pp. 2319–6483, 2013, [Online]. Available: https://pdfs.semanticscholar.org/74d0/667d71781962fc8f51a264bc6ecb7c270ba4.pdf.

[13] D. Gray, J. W. Lu, and D. V. Thiel, “Electronically steerable yagi-uda microstrip patch antenna array,” *IEEE Trans. Antennas Propag.*, vol. 46, no. 5, pp. 605–608, 1998, doi: 10.1109/8.668900.

[14] S. Gaya, O. Sokunbi, A. Hamza, S. I. M. Sheikh, and H. Attia, “Multiple-input-multiple-output antenna with pattern reconfiguration and correlation reduction for WLAN applications,” *Eng. Reports*, no. July, pp. 1–15, 2020, doi: 10.1002/eng2.12272.

[15] S. Gaya, R. Hussain, M. S. Sharawi, and H. Attia, “Pattern reconfigurable Yagi-Uda antenna with seven switchable beams for WiMAX application,” *Microw. Opt. Technol. Lett.*, vol. 62, no. 3, pp. 1329–1334, 2020, doi: 10.1002/mop.32147.

[16] D. Rodrigo, J. Romeu, B. A. Cetiner, and L. Jofre, “Pixel reconfigurable antennas: Towards low-complexity full reconfiguration,” *2016 10th Eur. Conf. Antennas Propagation, EuCAP 2016*, no. March 2018, 2016, doi: 10.1109/EuCAP.2016.7481208.

[17] Z. Li, H. Mopidevi, O. Kaynar, and B. A. Cetiner, “Beam-steering antenna

based on parasitic layer," *Electron. Lett.*, vol. 48, no. 2, pp. 59–60, 2012, doi: 10.1049/el.2011.2787.

[18] L. Ukkonen, L. Sydänheimo, and M. Kivikoski, "Effects of metallic plate size on the performance of microstrip patch-type tag antennas for passive RFID," *IEEE Antennas Wirel. Propag. Lett.*, vol. 4, no. 1, pp. 410–413, 2005, doi: 10.1109/LAWP.2005.860212.

[19] Y. Liu *et al.*, "Some recent developments of microstrip antenna," *Int. J. Antennas Propag.*, vol. 2012, 2012, doi: 10.1155/2012/428284.

[20] N. Ripin, R. A. Awang, A. A. Sulaiman, N. H. Baba, and S. Subahir, "Rectangular microstrip patch antenna with EBG structure," *SCOReD 2012 - 2012 IEEE Student Conf. Res. Dev.*, pp. 266–271, 2012, doi: 10.1109/SCOReD.2012.6518651.

[21] Cisco, "Antenna Pattern and Meaning," pp. 1–17, 2007, [Online]. Available: https://www.industrialnetworking.com/pdf/Antenna-Patterns.pdf.

[22] C. Larsson, "Access Networks," *5G Networks*, pp. 203–222, 2018, doi: 10.1016/b978-0-12-812707-0.00014-0.

[23] K. F. Lee and K. M. Luk, *Microstrip Patch Antennas*. 2010.

[24] T. A. Milligan, *Modern Antenna Design*. 2005.

[25] S. I. Toos, "Voltage Standing Wave Ratio_Baidu Baike," no. December 2010, 2019, [Online]. Available: https://baike.baidu.com/item/电压驻波比.

[26] J. Rahola, "Estimating antenna bandwidth using the bandwidth potential and Q value techniques," pp. 0–3.

[27] A. D. Yaghjian and S. R. Best, "Impedance, bandwidth, and Q of antennas," *IEEE Trans. Antennas Propag.*, vol. 53, no. 4, pp. 1298–1324, 2005, doi: 10.1109/TAP.2005.844443.

[28] G. Ab, "GPR Antenna Bandwidth," 2006, [Online]. Available:

http://www.geoscanners.com/pdf/gprbw.pdf.

[29] U. Keskin, B. Döken, and M. Kartal, “Bandwidth improvement in microstrip patch antenna,” *Proc. 8th Int. Conf. Recent Adv. Sp. Technol. RAST 2017*, pp. 215–219, 2017, doi: 10.1109/RAST.2017.8003005.

[30] Y. Lee, S. Tse, Y. Hao, and C. G. Parini, “A compact microstrip antenna with improved bandwidth using complementary split-ring resonator (CSRR) loading,” *IEEE Antennas Propag. Soc. AP-S Int. Symp.*, no. d, pp. 5431–5434, 2007, doi: 10.1109/APS.2007.4396776.

[31] S. Bisht, S. Saini, V. Prakash, and B. Nautiyal, “Study The Various Feeding Techniques of Microstrip Antenna Using Design and Simulation Using CST Microwave Studio,” *Int. J. Emerg. Technol. Adv. Eng.*, vol. 4, no. 9, pp. 318–324, 2014.

[32] and A. Constantine A. Balanis, "Microstrip Antennas: Analysis, Design, *Antenna Theroy BALANIS*. 2005.

[33] M. Kapoor, “CHAPTER -3 Electromagnetic BandGap Structures,” *Ph.D. Diss. Dayalbagh Educ. Institute, Agra, India*, pp. 34–56, 2013.

[34] L. Yang, M. Fan, F. Chen, J. She, and Z. Feng, “A novel compact electromagnetic-bandgap (EBG) structure and its applications for microwave circuits,” *IEEE Trans. Microw. Theory Tech.*, vol. 53, no. 1, pp. 183–189, 2005, doi: 10.1109/TMTT.2004.839322.

[35] D. Qu, “ENHANCEMENT OF MICRO STRIP ANTENNAS PERFORMANCE USING ELECTROMAGINETIC Master of Science,” University of Manitoba, 2004.

[36] H. Kim, K. B. Yeon, W. Kim, and C. S. Park, “Design and implementation of electromagnetic band-gap embedded antenna for vehicle-to-everything communications in vehicular systems,” *ETRI J.*, vol. 41, no. 6, pp. 731–738, 2019, doi: 10.4218/etrij.2017-0197.

[37] F. Yang and Y. Rahmat-Samii, “Microstrip Antennas Integrated with Electromagnetic Band-Gap (EBG) Structures: A Low Mutual Coupling Design for Array Applications,” *IEEE Trans. Antennas Propag.*, vol. 51, no. 10 II, pp. 2936–2946, 2003, doi: 10.1109/TAP.2003.817983.

[38] X. Zhang, Z. Teng, Z. Liu, and B. Li, “A dual band patch antenna with a pinwheel-shaped slots EBG substrate,” *Int. J. Antennas Propag.*, vol. 2015, 2015, doi: 10.1155/2015/815751.

[39] D. Nashaat, H. A. Elsadek, E. A. Abdallah, M. F. Iskander, and H. M. Elhenawy, “Ultrawide bandwidth 2 × 2 microstrip patch array antenna using electromagnetic band-gap structure (EBG),” *IEEE Trans. Antennas Propag.*, vol. 59, no. 5, pp. 1528–1534, 2011, doi: 10.1109/TAP.2011.2123052.

[40] “[P._Bhartia,_Inder_Bahl,_R._Garg,_A._Ittipiboon]_M(BookFi.org).pdf.” .

[41] P. Kovács, “Design and Optimization of Electromagnetic Band Gap Structures,” *Thesis*, 2012, [Online]. Available: http://dspace.vutbr.cz/xmlui/handle/11012/599.

[42] S. Akkole and V. N, “Square microstrip multi band fractal antenna using EBG structure for wireless applications,” *Int. J. Pervasive Comput. Commun.*, 2020, doi: 10.1108/IJPCC-08-2019-0062.

[43] L. C. Godara, “Smart antennas,” *Smart Antennas*, pp. 1–449, 2004, doi: 10.1002/ett.4460120502.

[44] S. Bellofiore, J. Foutz, C. A. Balanis, and A. Spanias, “Smart antennas for wireless communications,” *IEEE Antennas Propag. Soc. Int. Symp.*, no. January, pp. 26–29, 2001, [Online]. Available: http://123seminarsonly.com/Seminar-Reports/050/109618796-Smart-Antennas.pdf.

[45] Gilbert, “Application of Smart Antennas To Mobile Communications,” pp. 53–76, 2010.

[46] G. Misra, K. Agarwal, A. Agarwal, K. Ghosh, and S. Agarwal, “Smart antenna for wireless cellular communication-a technological analysis on architecture, working mechanism, drawbacks and future scope,” *Proc. Int. Conf. I-SMAC (IoT Soc. Mobile, Anal. Cloud), I-SMAC 2018*, no. February, pp. 37–41, 2019, doi: 10.1109/I-SMAC.2018.8653711.

[47] P. Vallese, N. Varanese, and U. Spagnolini, “Self-interference cancellation for multi-antenna full duplex radio systems,” *21st Int. ITG Work. Smart Antennas, WSA 2017*, pp. 341–346, 2017.

[48] A. Goldsmith, *Wireless communications*. Cambridge University Press, 2005.

[49] D. Bharadia, E. McMilin, and S. Katti, “Full duplex radios,” *SIGCOMM 2013 - Proc. ACM SIGCOMM 2013 Conf. Appl. Technol. Archit. Protoc. Comput. Commun.*, pp. 375–386, 2013, doi: 10.1145/2486001.2486033.

[50] M. Franco-Martínez, F.-J. Martínez-Alonso, and R. López-Valcarce, “Solving Self-Interference Issues in a Full-Duplex Radio Transceiver,” *Proceedings*, vol. 21, no. 1, p. 35, 2019, doi: 10.3390/proceedings2019021035.

[51] S. Ahmadi *et al.*, “pects (Part 1) New Radio Access Physical Layer As- Self-Interference.”

[52] J. Il Choi, M. Jain, K. Srinivasan, P. Levis, and S. Katti, “Achieving Single Channel, Full Duplex Wireless Communication,” in *MobiCom ’10: Proceedings of the sixteenth annual international conference on Mobile computing and networking*, 2010, vol. 78, no. 2–3, pp. 1–12, doi: 10.1145/1859995.1859997.

[53] H. Nawaz and I. Tekin, “Dual polarized patch antenna with high inter-port isolation for 1GHz in-band full Duplex applications,” *2016 IEEE Antennas Propag. Soc. Int. Symp. APSURSI 2016 - Proc.*, pp. 2153–2154, 2016, doi: 10.1109/APS.2016.7696783.

[54] S. Bojja-Venkatakrishnan, E. A. Alwan, and J. L. Volakis, “Wideband RF and

analog self-interference cancellation filter for simultaneous transmit and receive system," *2017 IEEE Antennas Propag. Soc. Int. Symp. Proc.*, vol. 2017-Janua, pp. 933–934, 2017, doi: 10.1109/APUSNCURSINRSM.2017.8072509.

[55] T. Nesimoglu, Z. Charalampopoulos, P. A. Warr, and M. A. Beach, "Dynamic range enhancements in radio receivers by means of frequency retranslation," *IET Microwaves, Antennas Propag.*, vol. 6, no. 4, pp. 489–496, 2012, doi: 10.1049/iet-map.2010.0558.

[56] Z. Rahimi, "The Finite Integration Technique (FIT) and the Application in Lithography Simulations," p. 132, 2011.

[57] M. C. Tang, B. Zhou, Y. Duan, X. Chen, and R. W. Ziolkowski, "Pattern-Reconfigurable, Flexible, Wideband, Directive, Electrically Small Near-Field Resonant Parasitic Antenna," *IEEE Trans. Antennas Propag.*, vol. 66, no. 5, pp. 2271–2280, 2018, doi: 10.1109/TAP.2018.2814220.

[58] R. Ahmadian, F. B. Zarrabi, and Z. Mansouri, "Investigation of EBG array performance on decreasing the mutual coupling and improve shield factor," *J. Electr. Syst. Inf. Technol.*, vol. 2, no. 2, pp. 184–196, 2015, doi: 10.1016/j.jesit.2015.06.001.

[59] M. I. Skolnik, *Radar Hanbook*, vol. 53. 1990.

[60] M. K. Abdulhameed, M. S. M. Isa, I. M. Ibrahim, Z. Zakaria, and M. K. Mohsen, "Side lobe reduction in array antenna by using novel design of EBG," 2020, doi: 10.11591/ijece.v10i1.pp308-315.

APPENDICES

A. Beam Steering of 2x2 antenna array without EBG

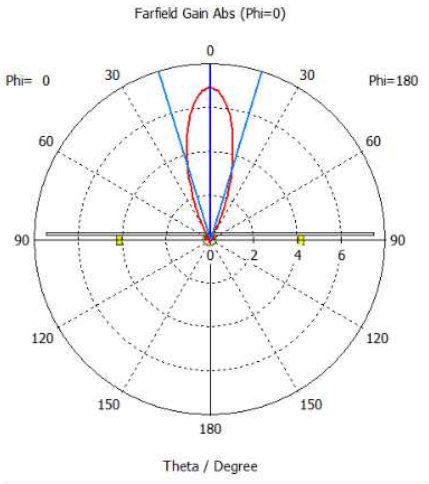

(a) 0° beam steering

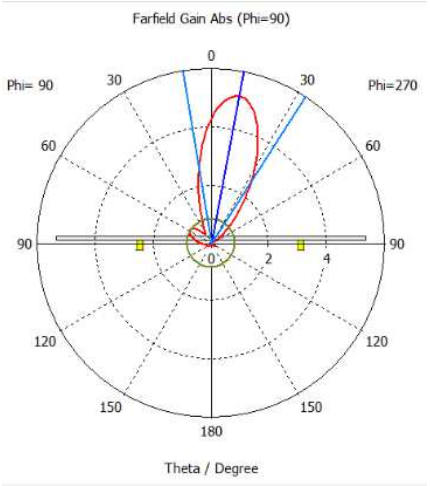

(b) -11° beam steering

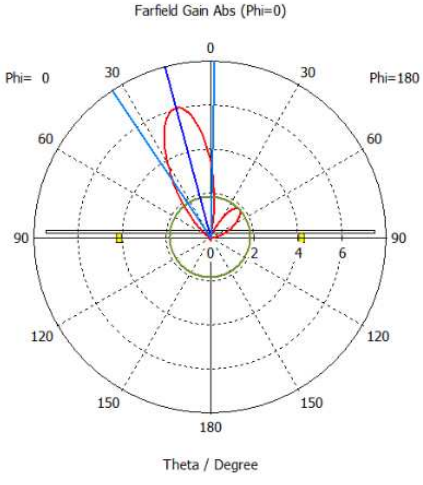

(c) 15° beam steering

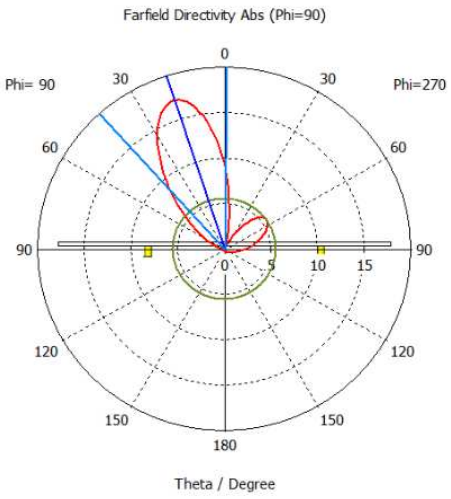

(d) 18° beam steering

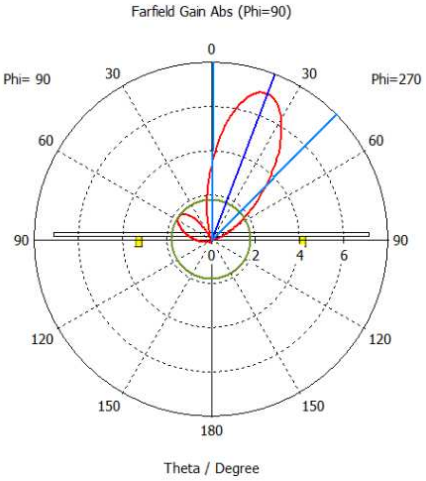

(a) -21° beam steering

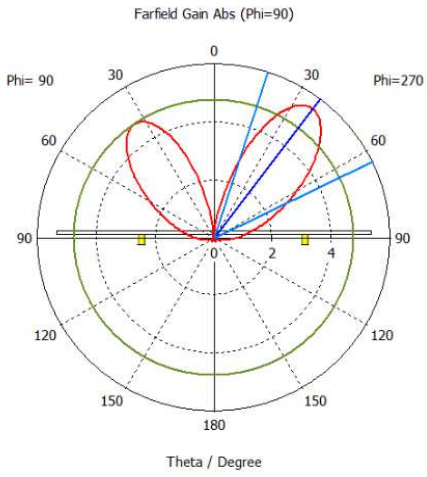

(a) ±36° beam steering

Figure 5.1 Polar plots of the 2x2 antenna array without EBG showing beam steering from -36° to 36

B. Far-field pattern of the 2x2 antenna array with increasing phase shifts on Port 1

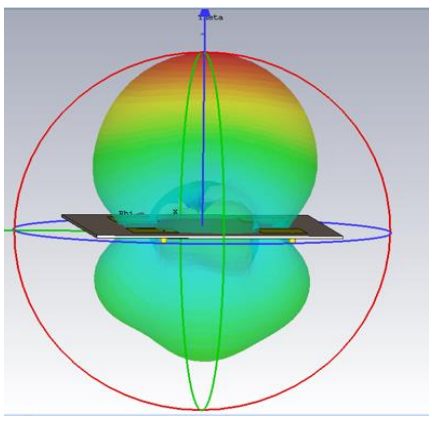

a)

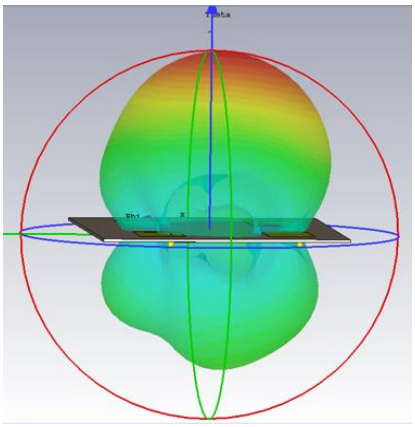

b)

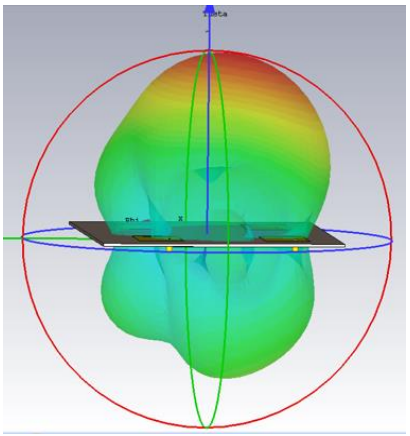

c)

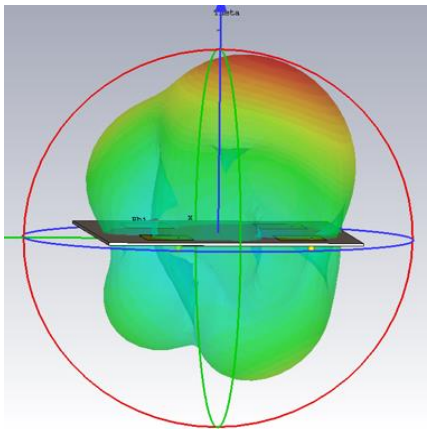

d)

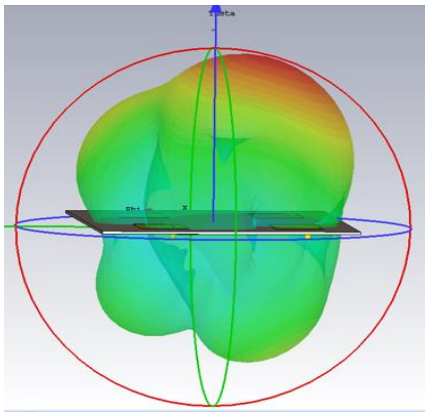

e)

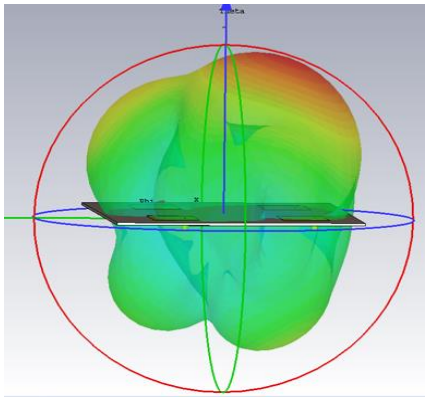

f)

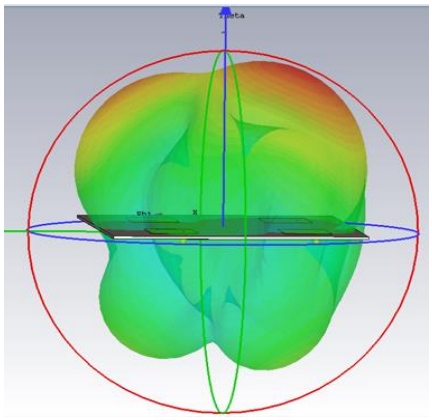

g)

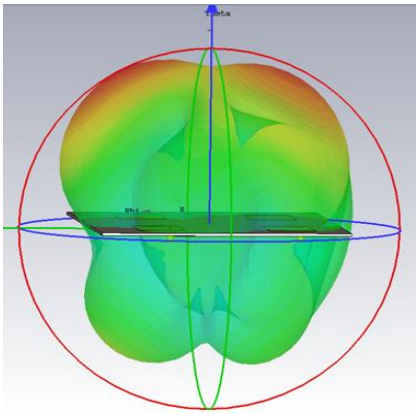

h)

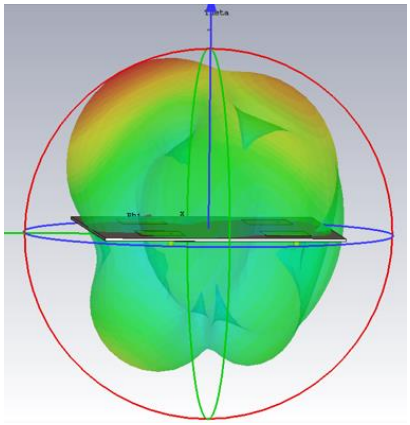

i)

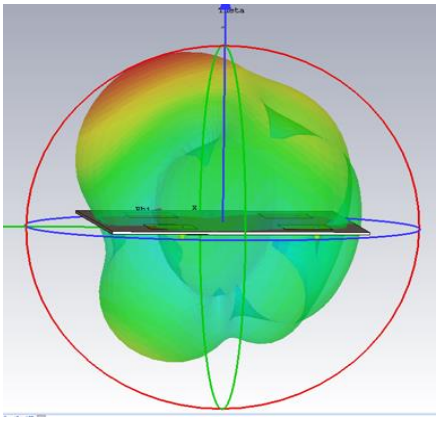

j)

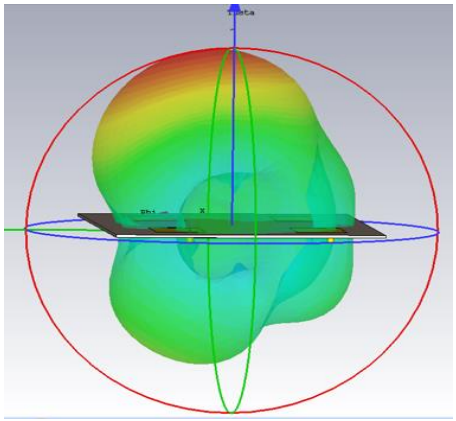

k)

Figure 5.2 Resulting far-field result for all ports excitation with 10° to 300° phase shifts in port 1; a) 10°, b) 30°, c) 50°, d) 90°, e) 100°, f) 120°, g) 150°, h) 180°, i) 200°, j) 230°, k) 300°

C. SMP1345-040LF PIN-diode datasheet

SKYWORKS®

DATA SHEET

SMP1345 Series: Very Low Capacitance, Plastic Packaged Silicon PIN Diodes

Applications

- High isolation LNBs, WLANs, and wireless switches

Features

- Very low insertion loss: 0.4 dB
- Capacitance: 0.15 pF
- Packages rated MSL1, 260 °C per JEDEC J-STD-020

Skyworks Green™ products are compliant with all applicable legislation and are halogen-free. For additional information, refer to *Skyworks Definition of Green™*, document number SQ04–0074.

Description

The SMP1345 series of plastic packaged, surface mountable PIN diodes is designed for high volume Low-Noise Block (LNB), Wireless Local Area Network (WLAN), and switch applications from 10 MHz to 6 GHz. The short carrier lifetime of 100 ns (typical), combined with their thin I-region width of 10 µm (nominal) results in a group of fast speed RF switching PIN diodes.

The RF performance of the SMP1345 series is assured by virtue of their very low capacitance (0.15 pF) and low resistance (1.5 Ω at 10 mA).

Table 1 describes the various packages and marking of the SMP1345 series.

Table 1. SMP1345 Series Packaging and Marking

		
Common Cathode	Single	Single
SOT-23	SC-79 Green™	SOD-882 Green™
SMP1345-004LF Green™ Marking: RU3	**SMP1345-079LF** Marking: Cathode and CF	**SMP1345-040LF** Marking: U
L_S = 1.5 nH	L_S = 0.7 nH	L_S = 0.45 nH

Electrical and Mechanical Specifications

The absolute maximum ratings of the SMP1345 series are provided in Table 2. Electrical specifications are provided in Table 3.

Typical performance characteristics of the SMP1345 series are illustrated in Figures 1 through 6.

Table 2. SMP1345 Series Absolute Maximum Ratings[1]

Parameter	Symbol	Minimum	Maximum	Units
Reverse voltage	V_R		50	V
Power dissipation @ 25 °C lead temperature	P_D		250	mW
Storage temperature	T_{STG}	-65	+150	°C
Operating temperature	T_A	-65	+150	°C
Electrostatic discharge:	ESD			
Human Body Model (HBM), Class 1B			1000	V

[1] Exposure to maximum rating conditions for extended periods may reduce device reliability. There is no damage to device with only one parameter set at the limit and all other parameters set at or below their nominal value. Exceeding any of the limits listed here may result in permanent damage to the device.

ESD HANDLING: *Although this device is designed to be as robust as possible, electrostatic discharge (ESD) can damage this device. This device must be protected at all times from ESD when handling or transporting. Static charges may easily produce potentials of several kilovolts on the human body or equipment, which can discharge without detection. Industry-standard ESD handling precautions should be used at all times.*

Table 3. SMP1345 Series Electrical Specifications[1]
(T_A = +25 °C, Unless Otherwise Noted)

Parameter	Symbol	Test Condition	Min	Typ	Max	Units
Reverse current	I_R	V_R = 50 V			10	µA
Capacitance	C_T	F = 1 MHz:				
		V = 1 V		0.19		pF
		V = 5 V		0.18	0.20	pF
Resistance	R_S	F = 100 MHz:				
		I = 1 mA		3.5		Ω
		I = 10 mA		1.5	2.0	Ω
Forward voltage	V_F	I_F = 10 mA		0.89		V
Carrier lifetime	TI	I_F = 10 mA		100		ns
I region width				10		µm

[1] Performance is guaranteed only under the conditions listed in this table.

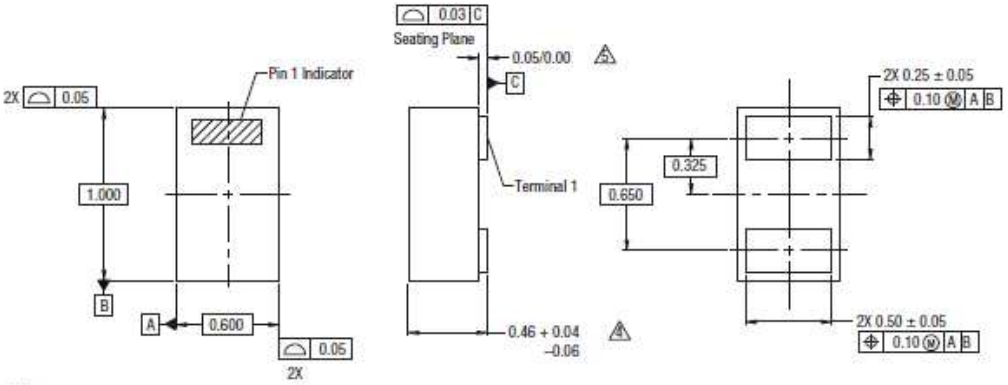

Notes:

1. All measurements are in millimeters.
2. Dimensions and tolerances according to ASME Y14.5M-1994.
3. These packages are used principally for discrete devices.
4. This dimension includes stand-off height and package body thickness, but does not include attached features, e.g., external heatsink or chip capacitors. An integral heatslug is not considered an attached feature.
5. This dimension is primarily terminal plating, but does not include small metal protrusion.

200046-011

Figure 11. SOD-882 Package Dimension Drawing

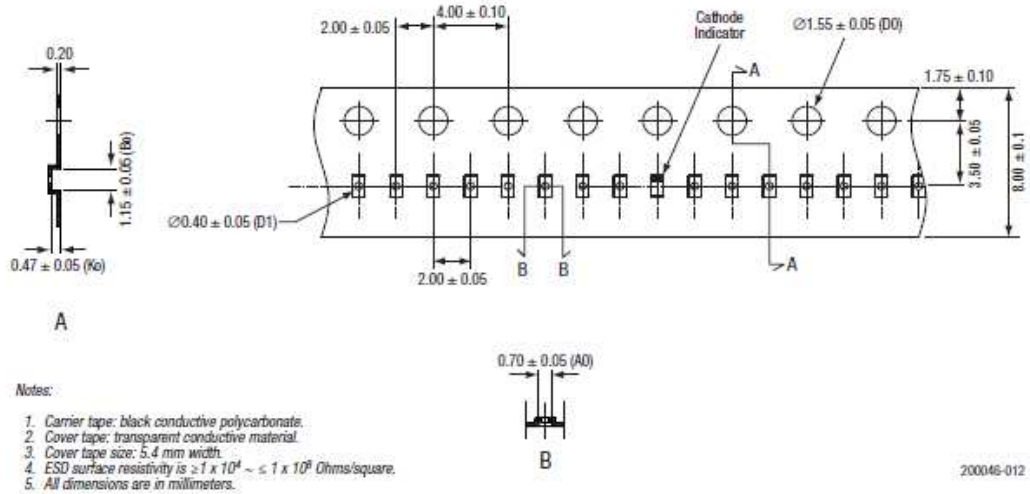

Notes:

1. Carrier tape: black conductive polycarbonate.
2. Cover tape: transparent conductive material.
3. Cover tape size: 5.4 mm width.
4. ESD surface resistivity is $\geq 1 \times 10^4 \sim \leq 1 \times 10^8$ Ohms/square.
5. All dimensions are in millimeters.

200046-012

Figure 12. SOD-882 Tape and Reel Drawing